

Covariance Matrix Adaptation MAP-Annealing

Matthew C. Fontaine
University of Southern California
Los Angeles, CA, USA
mfontain@usc.edu

Stefanos Nikolaidis
University of Southern California
Los Angeles, CA, USA
nikolaid@usc.edu

ABSTRACT

Single-objective optimization algorithms search for the single highest-quality solution with respect to an objective. Quality diversity (QD) optimization algorithms, such as Covariance Matrix Adaptation MAP-Elites (CMA-ME), search for a collection of solutions that are both high-quality with respect to an objective and diverse with respect to specified measure functions. However, CMA-ME suffers from three major limitations highlighted by the QD community: prematurely abandoning the objective in favor of exploration, struggling to explore flat objectives, and having poor performance for low-resolution archives. We propose a new quality diversity algorithm, Covariance Matrix Adaptation MAP-Annealing (CMA-MAE), that addresses all three limitations. We provide theoretical justifications for the new algorithm with respect to each limitation. Our theory informs our experiments, which support the theory and show that CMA-MAE achieves state-of-the-art performance and robustness.

ACM Reference Format:

Matthew C. Fontaine and Stefanos Nikolaidis. 2023. Covariance Matrix Adaptation MAP-Annealing. In *Genetic and Evolutionary Computation Conference (GECCO '23)*, July 15–19, 2023, Lisbon, Portugal. ACM, New York, NY, USA, 36 pages. <https://doi.org/10.1145/3583131.3590389>

1 INTRODUCTION

Consider an example problem of searching for celebrity faces in the latent space of a generative model. As a single-objective optimization problem, we specify an objective f that targets a celebrity such as Tom Cruise. A single-objective optimizer, such as CMA-ES [35], will converge to a single solution of high objective value, an image that looks like Tom Cruise as much as possible.

However, this objective has ambiguity. How old was Tom Cruise in the photo? Did we want the person in the image to have short or long hair? By instead framing the problem as a quality diversity optimization problem, we additionally specify a measure function m_1 that quantifies age and a measure function m_2 that quantifies hair length. A quality diversity algorithm [8, 66], such as CMA-ME [26], can then optimize for a collection of images that are diverse with respect to age and hair length, but all look like Tom Cruise.

While prior work [17, 20, 24, 26] has shown that CMA-ME solves such QD problems efficiently, three important limitations of the algorithm have been discovered. First, on difficult to optimize objectives, variants of CMA-ME will abandon the objective too soon [76], and instead favor exploring the measure space, the vector space defined

by the measure function outputs. Second, the CMA-ME algorithm struggles to explore flat objective functions [62]. Third, CMA-ME works well on high-resolution archives, but struggles to explore low-resolution archives [14, 21].¹

We propose a new algorithm, CMA-MAE, that addresses these three limitations. To address the first limitation, we derive an algorithm that smoothly blends between CMA-ES and CMA-ME. First, consider how CMA-ES and CMA-ME differ. At each step CMA-ES's objective ranking maximizes the objective function f by approximating the natural gradient of f at the current solution point [1]. In contrast, CMA-ME's improvement ranking moves in the direction of the natural gradient of $f - f_A$ at the current solution point, where f_A is a discount function equal to the objective of the best solution so far that has the same measure values as the current solution point. The function $f - f_A$ quantifies the gap between a candidate solution and the best solution so far at the candidate solution's position in measure space.

Our key insight is to *anneal the function f_A by a learning rate α* . We observe that when $\alpha = 0$, then our discount function f_A never increases and our algorithm behaves like CMA-ES. However, when $\alpha = 1$, then our discount function always maintains the best solution for each region in measure space and our algorithm behaves like CMA-ME. For $0 < \alpha < 1$, CMA-MAE smoothly blends between the two algorithms' behavior, allowing for an algorithm that spends more time on the optimization of f before transitioning to exploration. Figure 1 is an illustrative example of varying the learning rate α .

Our proposed annealing method naturally addresses the flat objective limitation. Observe that both CMA-ES and CMA-ME struggle on flat objectives f as the natural gradient becomes 0 in this case and each algorithm will restart. However, we show that, when CMA-MAE optimizes $f - f_A$ for $0 < \alpha < 1$, the algorithm becomes a descent method on the density histogram defined by the archive.

Finally, CMA-ME's poor performance on low resolution archives is likely caused by the non-stationary objective $f - f_A$ changing too quickly for the adaptation mechanism to keep up. Our archive learning rate α controls how *quickly* $f - f_A$ changes. We derive a conversion formula for α that allows us to derive equivalent α for different archive resolutions. Our conversion formula guarantees that CMA-MAE is the first QD algorithm invariant to archive resolution.

While our new annealing method benefits CMA-ME, our approach is also compatible with CMA-ME's differentiable quality diversity (DQD) counterpart, CMA-MEGA [21]. We apply the same modification in the DQD setting to form CMA-MAEGA. To evaluate CMA-MAEGA, we improve the latent space illumination (LSI) [21] domain by introducing a higher-dimensional domain based on StyleGAN2, capable of producing higher quality images. This new domain highlights the advantages of DQD in high-dimensional spaces and demonstrates the performance benefits of our annealing method.

¹We note that archive resolution affects the performance of all current QD algorithms.

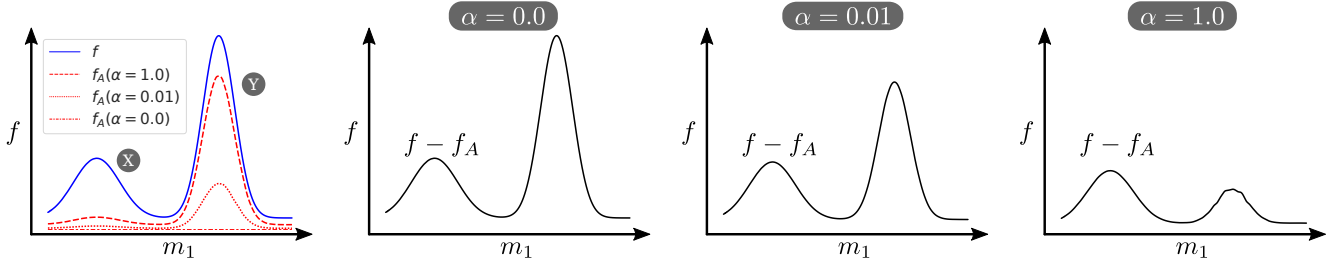


Figure 1: An example of how different α values affect the function $f - f_A$ optimized by CMA-MAE after a fixed number of iterations. Here f is a bimodal objective where mode X is harder to optimize than mode Y , requiring more optimization steps, and modes X and Y are separated by measure m_1 . For $\alpha = 0$, the objective f is equivalent to $f - f_A$, as f_A remains constant. For larger values of α , CMA-MAE discounts region Y in favor of prioritizing the optimization of region X .

Overall, our work shows how a simple algorithmic change to CMA-ME addresses all three major limitations affecting CMA-ME’s performance and robustness. Our theoretical findings justify the aforementioned properties and inform our experiments, which show that CMA-MAE outperforms state-of-the-art QD algorithms and maintains robust performance across different archive resolutions.

2 PROBLEM DEFINITION

Quality Diversity. We adopt the quality diversity (QD) problem definition from prior work [21]. A QD problem consists of an objective function $f : \mathbb{R}^n \rightarrow \mathbb{R}$ that maps n -dimensional solution parameters to the scalar value representing the quality of the solution and k measure functions $m_i : \mathbb{R}^n \rightarrow \mathbb{R}$ or, as a vector function, $\mathbf{m} : \mathbb{R}^n \rightarrow \mathbb{R}^k$ that quantify the behavior or attributes of each solution.² The range of \mathbf{m} forms a measure space $S = \mathbf{m}(\mathbb{R}^n)$. The QD objective is to find a set of solutions $\theta \in \mathbb{R}^n$, such that $\mathbf{m}(\theta) = s$ for each s in S and $f(\theta)$ is maximized.

The measure space S is continuous, but solving algorithms need to produce a finite collection of solutions. Therefore, QD algorithms in the MAP-Elites [15, 59] family relax the QD objective by discretizing the space S . Given T as the tessellation of S into M cells, the QD objective becomes to find a solution θ_i for each of the $i \in \{1, \dots, M\}$ cells, such that each θ_i maps to the cell corresponding to $\mathbf{m}(\theta_i)$ in the tessellation T . The QD objective then becomes maximizing the objective value $f(\theta_i)$ of all cells:

$$\max \sum_{i=1}^M f(\theta_i) \quad (1)$$

The *differentiable quality diversity* (DQD) problem [21] is a special case of the QD problem where both the objective f and measures m_i are *first-order differentiable*.

3 PRELIMINARIES

We present several QD algorithms that solve derivative-free QD problems to provide context for our proposed CMA-MAE algorithm. Appendix D contains information about the DQD algorithm CMA-MEGA, which solves problems where the gradients of the objective and measure functions are available.

²In agent-based settings, such as reinforcement learning, the measure functions are sometimes called behavior functions and the outputs of each measure function are called behavioral characteristics or behavior descriptors.

MAP-Elites and MAP-Elites (line). The MAP-Elites QD algorithm produces an archive of solutions, where each cell in the archive corresponds to the provided tessellation T in the QD problem definition. The algorithm initializes the archive by sampling solutions from the solution space \mathbb{R}^n from a fixed distribution. After initialization, MAP-Elites produces new solutions by selecting occupied cells uniformly at random and perturbing them with isotropic Gaussian noise: $\theta' = \theta_i + \sigma \mathcal{N}(0, I)$. For each new candidate solution θ' , the algorithm computes an objective $f(\theta')$ and measures $\mathbf{m}(\theta')$. MAP-Elites places θ' into the archive if the cell corresponding to $\mathbf{m}(\theta')$ is empty or θ' obtains a better objective value $f(\theta')$ than the current occupant. The MAP-Elites algorithm results in an archive of solutions that are diverse with respect to the measure function \mathbf{m} , but also high quality with respect to the objective f . Prior work [79] proposed the MAP-Elites (line) algorithm by augmenting the isotropic Gaussian perturbation with a linear interpolation between two solutions θ_i and θ_j : $\theta' = \theta_i + \sigma_1 \mathcal{N}(0, I) + \sigma_2 \mathcal{N}(0, 1)(\theta_i - \theta_j)$. **CMA-ME.** Covariance Matrix Adaptation MAP-Elites [26] combines the archiving mechanisms of MAP-Elites with the adaptation mechanisms of CMA-ES [35]. Instead of perturbing archive solutions with Gaussian noise, CMA-ME maintains a multivariate Gaussian of search directions $\mathcal{N}(0, \Sigma)$ and a search point $\theta \in \mathbb{R}^n$. The algorithm updates the archive by sampling λ solutions around the current search point $\theta_i \sim \mathcal{N}(\theta, \Sigma)$. After updating the archive, CMA-ME ranks solutions via a two stage ranking. Solutions that discover a new cell are ranked by the objective $\Delta_i = f(\theta_i)$, and solutions that map to an occupied cell e are ranked by the improvement over the incumbent solution θ_e in that cell: $\Delta_i = f(\theta_i) - f(\theta_e)$. CMA-ME prioritizes exploration by ranking all solutions that discover a new cell before all solutions that improve upon an existing cell. Finally, CMA-ME moves θ towards the largest improvement in the archive, according to the CMA-ES update rules. Prior work [21] showed that the improvement ranking of CMA-ME approximates a natural gradient of a modified QD objective (see Eq. 1).

4 PROPOSED ALGORITHMS

We present the CMA-MAE algorithm. While we focus on CMA-MAE, the same augmentations apply to CMA-MEGA to form the novel CMA-MAEGA algorithm (see Appendix D).

CMA-MAE. CMA-MAE is an algorithm that adjusts the rate the non-stationary QD objective $f - f_A$ changes. First, consider at a

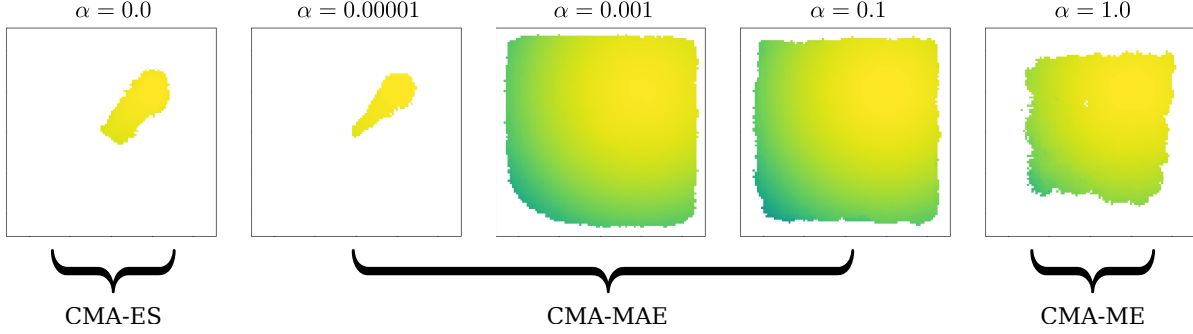


Figure 2: Our proposed CMA-MAE algorithm smoothly blends between the behavior of CMA-ES and CMA-ME via an archive learning rate α . Each heatmap visualizes an archive of solutions across a 2D measure space, where the color of each cell represents the objective value of the solution.

high level how CMA-ME explores the measure space and discovers high quality solutions. The CMA-ME algorithm maintains a solution point θ and an archive A with previously discovered solutions. When CMA-ME samples a new solution θ' , the algorithm computes the solution's objective value $f(\theta')$ and maps the solution to a cell e in the archive based on the measure $\mathbf{m}(\theta')$. CMA-ME then computes the improvement of the objective value $f(\theta')$ of the new solution, over a discount function $f_A : \mathbb{R}^n \rightarrow \mathbb{R}$. In CMA-ME, we define $f_A(\theta')$ by computing the cell e in the archive corresponding to $\mathbf{m}(\theta')$ and letting $f_A(\theta') = f(\theta_e)$, where θ_e is the incumbent solution of cell e . The algorithm ranks candidate solutions by improvement $f(\theta') - f_A(\theta') = f(\theta') - f(\theta_e)$ and moves the search in the direction of higher ranked solutions.

Assume that CMA-ME samples a new solution θ' with a high objective value of $f(\theta') = 99$. If the current occupant θ_e of the corresponding cell has a low objective value of $f(\theta_e) = 0.3$, then the improvement in the archive $\Delta = f(\theta') - f(\theta_e) = 98.7$ is high and the algorithm will move the search point θ towards θ' . Now, assume that in the next iteration the algorithm discovers a new solution θ'' with objective value $f(\theta'') = 100$ that maps to the same cell as θ' . The improvement then is $\Delta = f(\theta'') - f(\theta') = 1$ as θ' replaced θ_e in the archive in the previous iteration. CMA-ME would likely move θ away from θ'' as the solution resulted in low improvement. In contrast, CMA-ES would move towards θ'' as it ranks only by the objective f , ignoring previously discovered solutions with similar measure values.

In the above example, CMA-ME moves away from a high performing region in order to maximize how the archive changes. However, in domains with hard-to-optimize objective functions, it is beneficial to perform more optimization steps towards the objective f before leaving each high-performing region [76].

Like CMA-ME, CMA-MAE maintains a discount function $f_A(\theta')$ and ranks solutions by improvement $f(\theta') - f_A(\theta')$. However, instead of maintaining an *elitist archive* by setting $f_A(\theta')$ equal to $f(\theta_e)$, we maintain a *soft archive* by setting $f_A(\theta')$ equal to t_e , where t_e is an acceptance threshold maintained for each cell in the archive A . When adding a candidate solution to the archive, we control the rate that t_e changes by the archive learning rate α as follows: $t_e \leftarrow (1 - \alpha)t_e + \alpha f(\theta')$.

The archive learning rate α in CMA-MAE allows us to control how quickly we leave a high-performing region of measure space. For example, consider discovering solutions in the same cell with objective value 100 in 5 consecutive iterations. The improvement values computed by CMA-ME against the elitist archive would be 100, 0, 0, 0, 0, thus CMA-ME would move rapidly away from this cell. The improvement values computed against the soft archive of CMA-MAE with $\alpha = 0.5$ would diminish smoothly as follows: 100, 50, 25, 12.5, 6.25, enabling further exploitation of the high-performing region.

Next, we walk through the CMA-MAE algorithm step-by-step. Algorithm 1 shows the pseudo-code for CMA-MAE with the differences from CMA-ME highlighted in yellow. First, on line 3 we initialize the acceptance threshold to \min_f . In each iteration we sample λ solutions around the current search point θ (line 6). For each candidate solution θ_i , we evaluate the solution and compute the objective value $f(\theta_i)$ and measure values $\mathbf{m}(\theta_i)$ (line 7). Next, we compute the cell e in the archive that corresponds to the measure values and the improvement Δ_i over the current threshold t_e (lines 8-9). If the objective crosses the acceptance threshold t_e , we replace the incumbent θ_e in the archive and increase the acceptance threshold t_e (lines 10-12). Next, we rank all candidate solutions θ_i by their improvement Δ_i . Finally, we step our search point θ and adapt our covariance matrix Σ towards the direction of largest improvement (lines 15-16) according to CMA-ES's update rules [35].

CMA-MAEGA. We note that our augmentations to the CMA-ME algorithm only affects how we replace solutions in the archive and how we calculate Δ_i . CMA-ME and CMA-MEGA replace solutions and calculate Δ_i identically, so we apply the same augmentations to CMA-MEGA to form a new DQD algorithm, CMA-MAEGA, in Appendix D.

5 THEORETICAL PROPERTIES OF CMA-MAE

We provide insights about the behavior of CMA-MAE for different α values. We include all proofs in Appendix E. CMA-MAEGA has similar theoretical properties discussed in Appendix F.

THEOREM 5.1. *The CMA-ES algorithm is equivalent to CMA-MAE when $\alpha = 0$, if CMA-ES restarts from an archive solution.*

```

1 CMA-MAE (evaluate,  $\theta_0$ ,  $N$ ,  $\lambda$ ,  $\sigma$ ,  $\min_f$ ,  $\alpha$ )
   input : An evaluation function evaluate that computes
           the objective and measures, an initial solution  $\theta_0$ ,
           a desired number of iterations  $N$ , a branching
           population size  $\lambda$ , an initial step size  $\sigma$ , a minimal
           acceptable solution quality  $\min_f$ , and an archive
           learning rate  $\alpha$ .
   result : Generate  $N\lambda$  solutions storing elites in an archive
           A.
2   Initialize solution parameters  $\theta$  to  $\theta_0$ , CMA-ES
   parameters  $\Sigma = \sigma I$  and  $p$ , where we let  $p$  be the
   CMA-ES internal parameters.
3   Initialize the archive A and the acceptance threshold  $t_e$ 
   with  $\min_f$  for each cell  $e$ .
4   for  $iter \leftarrow 1$  to  $N$  do
5       for  $i \leftarrow 1$  to  $\lambda$  do
6            $\theta_i \sim \mathcal{N}(\theta, \Sigma)$ 
7            $f, m \leftarrow \text{evaluate}(\theta_i)$ 
8            $e \leftarrow \text{calculate\_cell}(A, m)$ 
9            $\Delta_i \leftarrow f - t_e$ 
10          if  $f > t_e$  then
11              Replace the current occupant in cell  $e$  of the
              archive A with  $\theta_i$ 
12               $t_e \leftarrow (1 - \alpha)t_e + \alpha f$ 
13          end
14      end
15      rank  $\theta_i$  by  $\Delta_i$ 
16      Adapt CMA-ES parameters  $\theta, \Sigma, p$  based on
      improvement ranking  $\Delta_i$ 
17      if CMA-ES converges then
18          Restart CMA-ES with  $\Sigma = \sigma I$ .
19          Set  $\theta$  to a randomly selected existing cell  $\theta_i$  from
          the archive
20      end
21  end
    
```

Algorithm 1: Covariance Matrix Adaptation MAP-Annealing

The next theorem states that CMA-ME is equivalent to CMA-MAE when $\alpha = 1$ with the following caveats: First, we assume that CMA-ME restarts only by the CMA-ES restart rules, rather than the additional “no improvement” restart rule in prior work [26]. Second, we assume that both CMA-ME and CMA-MAE leverage μ selection [35] rather than filtering selection [26].

THEOREM 5.2. *The CMA-ME algorithm is equivalent to CMA-MAE when $\alpha = 1$ and \min_f is an arbitrarily large negative number.*

We next provide theoretical insights on how the discount function f_A smoothly increases from a constant function \min_f to the discount function used by CMA-ME, as α increases from 0 to 1. We focus on the special case of a fixed sequence of candidate solutions.

THEOREM 5.3. *Let α_i and α_j be two archive learning rates for archives A_i and A_j such that $0 \leq \alpha_i < \alpha_j \leq 1$. For two runs of CMA-MAE that generate the same sequence of m candidate solutions $\{S\} = \theta_1, \theta_2, \dots, \theta_m$, it follows that $f_{A_i}(\theta) \leq f_{A_j}(\theta)$ for all $\theta \in \mathbb{R}^n$.*

Finally, we wish to address the limitation that CMA-ME performs poorly on flat objectives, where all solutions have the same objective value. Consider how CMA-ME behaves on a flat objective $f(\theta) = C$ for all $\theta \in \mathbb{R}^n$, where C is an arbitrary constant. CMA-ME will only discover each new cell once and will not receive any further feedback from that cell, since any future solution cannot replace the incumbent elite. This hinders the CMA-ME’s movement in measure space, which is based on feedback from *changes* in the archive. Future candidate solutions will only fall into occupied cells, triggering repeated restarts caused by CMA-ES’s restart rule.

When the objective function plateaus, we still want CMA-ME to perform well and benefit from the CMA-ES adaptation mechanisms. One reasonable approach would be to keep track of the frequency o_e that each cell e has been visited in the archive, where o_e represents the number of times a solution was generated in that cell. Then, when a flat objective occurs, we rank solutions by descending frequency counts. Conceptually, CMA-ME would descend the density histogram defined by the archive, pushing the search towards regions of the measure space that have been sampled less frequently. Theorem 5.4 shows that we obtain the density descent behavior on flat objectives *without additional changes to the CMA-MAE algorithm*.

THEOREM 5.4. *The CMA-MAE algorithm optimizing a constant objective function $f(\theta) = C$ for all $\theta \in \mathbb{R}^n$ is equivalent to density descent, when $0 < \alpha < 1$ and $\min_f < C$.*

We highlight that the proof of Theorem 5.4 is based on two critical properties. First, the threshold update rule forms a strictly increasing sequence of thresholds for each cell. Second, CMA-ES is invariant to order preserving transformations of its objective f . While we have proposed the update rule of line 12 of Algorithm 1, we note that any update rule that satisfies the increasing sequence property retains the density descent property and is thus applicable in CMA-MAE.

While Theorem 5.4 assumes a constant objective f , we conjecture that the theorem holds true generally when threshold t_e in each cell e approaches the local optimum within the cell boundaries (see Conjecture E.7 in the Appendix).

6 EXPERIMENTS

We compare the performance of CMA-MAE with the state-of-the-art QD algorithms MAP-Elites, MAP-Elites (line), and CMA-ME, using existing Pyribs [77] QD library implementations. We set $\alpha = 0.01$ for CMA-MAE and include additional experiments for varying α in section 7. Because annealing methods replace solutions based on the threshold, we retain the best solution in each cell for comparison purposes. We include additional comparisons between CMA-MEGA and CMA-MAEGA – the DQD counterpart to CMA-MAE.

We select the benchmark domains from prior work [21]: linear projection [26], arm repertoire [16], and latent space illumination [24]. To evaluate the good exploration properties of CMA-MAE on flat objectives, we introduce a variant of the linear projection domain to include a “plateau” objective function that is constant everywhere for solutions within a fixed range and has a quadratic penalty for solutions outside the range. We describe the domains in detail in Appendix B.

We additionally introduce a second LSI experiment on StyleGAN2 [47], configured by insights from the generative art community [12, 27] that improve the quality of single-objective latent

	LP (sphere)		LP (Rastrigin)		LP (plateau)		Arm Repertoire		LSI (StyleGAN)		LSI (StyleGAN2)	
Algorithm	QD-score	Coverage	QD-score	Coverage	QD-score	Coverage	QD-score	Coverage	QD-score	Coverage	QD-score	Coverage
MAP-Elites	41.64	50.80%	31.43	47.88%	47.07	47.07%	71.40	74.09%	12.85	19.42%	-936.96	4.48%
MAP-Elites (line)	49.07	60.42%	38.29	56.51%	52.20	52.20%	74.55	75.61%	14.40	21.11%	-236.65	8.81%
CMA-ME	36.50	42.82%	38.02	53.09%	34.54	34.54%	75.82	75.89%	14.00	19.57%	—	—
CMA-MAE	64.86	83.31%	52.65	80.46%	79.27	79.29%	79.03	79.24%	17.67	25.08%	—	—

Table 1: Mean QD-score and coverage values after 10,000 iterations for each QD algorithm per domain.

	LP (sphere)		LP (Rastrigin)		LP (plateau)		Arm Repertoire		LSI (StyleGAN)		LSI (StyleGAN2)	
Algorithm	QD-score	Coverage	QD-score	Coverage	QD-score	Coverage	QD-score	Coverage	QD-score	Coverage	QD-score	Coverage
CMA-MEGA	75.32	100.00%	63.07	100.00%	100.00	100.00%	75.21	75.25%	16.08	22.58%	9.17	14.91%
CMA-MAEGA	75.39	100.00%	63.06	100.00%	100.00	100.00%	79.27	79.35%	16.20	23.83%	11.51	18.62%

Table 2: Mean QD-score and coverage values after 10,000 iterations for each DQD algorithm per domain.

space optimization. To improve control over image synthesis, the LSI (StyleGAN2) domain optimizes the full 9216-dimensional latent w -space, rather than a compressed 512-dimensional latent space in the LSI (StyleGAN) experiments. We exclude CMA-ME and CMA-MAE from this domain due to the prohibitive size of the covariance matrix. The LSI (StyleGAN2) domain allows us to evaluate the performance of DQD algorithms on a much more challenging DQD domain than prior work. We describe the domain in Appendix I.

6.1 Experiment Design

Independent Variables. We follow a between-groups design with two independent variables: the algorithm and the domain.

Dependent Variables. We use the sum of f values of all cells in the archive, defined as the QD-score [66], as a metric for the quality and diversity of solutions. Following prior work [21], we normalize the QD-score metric by the archive size (the total number of cells from the tessellation of measure space) to make the metric invariant to archive resolution. We additionally compute the coverage, defined as the number of occupied cells in the archive divided by the total number of cells.

6.2 Analysis

Derivative-free QD Algorithms. Table 1 shows the QD-score and coverage values for each algorithm and domain, averaged over 20 trials for the linear projection (LP) and arm repertoire domains and over 5 trials for the LSI domain. Fig. 3 shows the QD-score values for increasing number of iterations and example archives for CMA-MAE and CMA-ME with 95% confidence intervals.

We conducted a two-way ANOVA to examine the effect of the algorithm and domain on the QD-score. There was a significant interaction between the algorithm and the domain ($F(12, 320) = 1958.34, p < 0.001$). Simple main effects analysis with Bonferroni corrections showed that CMA-MAE outperformed all derivative-free QD baselines in all benchmark domains.

For the arm repertoire domain, we can compute the optimal archive coverage by testing whether each cell overlaps with a circle of radius equal to the maximum arm length (see Appendix B). We observe that CMA-MAE approaches the computed optimal coverage 80.24% for a resolution of 100×100 .

We observe from the runs that CMA-MAE initially explores regions of the measure space that have high-objective values. Once the archive becomes saturated, CMA-MAE reduces to approximate density descent, as we prove in Theorem 5.4 for flat objectives. On the other hand, CMA-ME does not receive any exploration signal when the objective landscape becomes flat, resulting in poor performance.

DQD Algorithms. We additionally compare CMA-MEGA and CMA-MAEGA in the five benchmark domains. Table 2 shows the QD-score and coverage values for each algorithm and domain, averaged over 20 trials for the linear projection (LP) and arm repertoire domains and over 5 trials for the LSI domains. We conducted a two-way ANOVA to examine the effect of the algorithm and domain on the QD-score. There was a significant interaction between the search algorithm and the domain ($F(5, 168) = 165.7, p < 0.001$). Simple main effects analysis with Bonferroni corrections showed that CMA-MAEGA outperformed CMA-MEGA in the LP (sphere), arm repertoire, and LSI (StyleGAN2) domains. There was no statistically significance difference between the two algorithms in the LP (Rastrigin), LP (plateau), and LSI (StyleGAN) domains.

We attribute the absence of a statistical difference in the QD-score between the two algorithms on the LP (Rastrigin) and LP (plateau) domains on the perfect coverage obtained by both algorithms. Thus, any differences in QD-score are based on the objective values of the solutions returned by each algorithm. In LP (plateau), the optimal objective for each cell is easily obtainable for both methods. The LP (Rastrigin) domain contains many local optima, because of the form of the objective function (Eq. 5). CMA-MEGA will converge to these optima before restarting, behaving as a single-objective optimizer within each local optimum. Because of the large number of local optima in the domain, CMA-MEGA obtains a higher QD-score.

In the LSI (StyleGAN) domain, we attribute similar performance between CMA-MEGA and CMA-MAEGA to the restart rules used to keep each search within the training distribution of StyleGAN. The ill-conditioned latent space of StyleGAN also explains why CMA-MAE outperforms both DQD algorithms on this domain. Being a natural gradient optimizer, CMA-MAE is an approximate second-order method, and second-order methods are better suited for optimizing spaces with ill-conditioned curvature.

On the other hand, in the LSI (StyleGAN2) domain, we regularize the search space by an L2 penalty in latent space, allowing for a

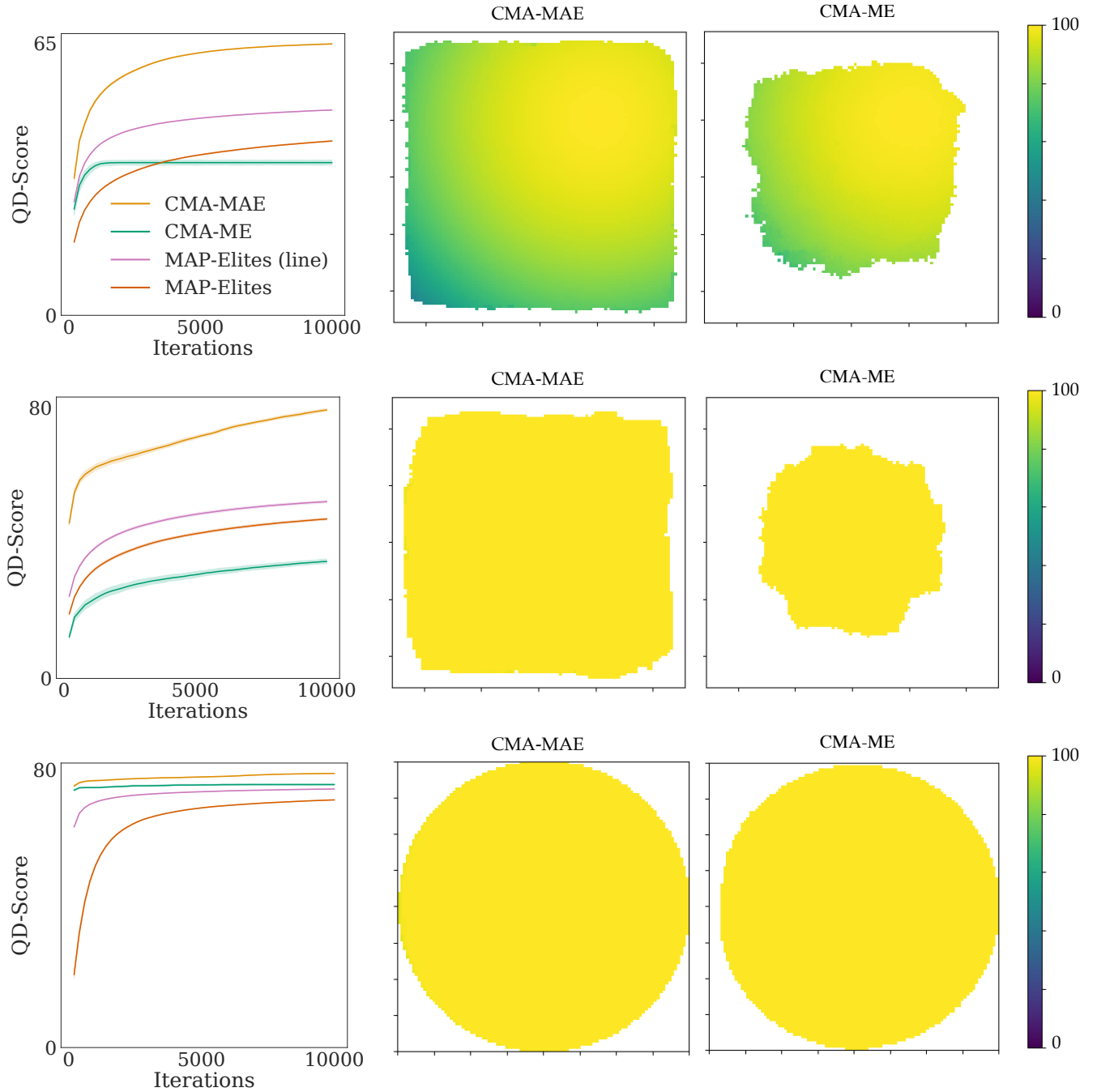


Figure 3: QD-score plot with 95% confidence intervals and heatmaps of generated archives by CMA-MAE and CMA-ME for the linear projection sphere (top), plateau (middle), and arm repertoire (bottom) domains. Each heatmap visualizes an archive of solutions across a 2D measure space.

larger learning rate and a basic restart rule for both algorithms, while still preventing drift out of the training distribution of StyleGAN2. Because of the fewer restarts, CMA-MAEGA can take advantage of the density descent property, which was shown to improve exploration in CMA-MAE, and outperform CMA-MEGA. Fig. 4 shows an

example collage generated from the final archive of CMA-MAEGA on the LSI (StyleGAN2) domain. We note that because StyleGAN2 has a better conditioning on the latent space [47], the model is better suited for first-order optimization of its latent space, which helps distinguish between the two QD algorithms.

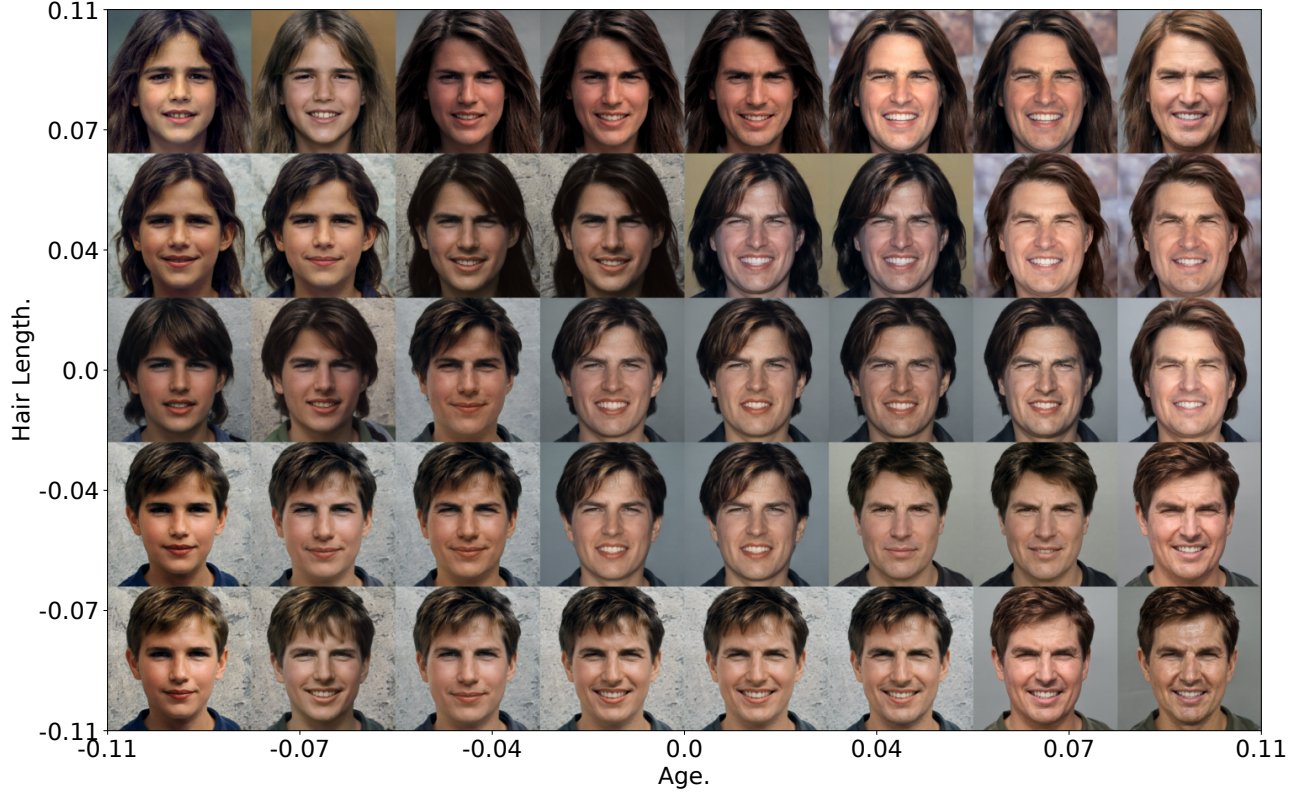


Figure 4: A latent space illumination collage for the objective “A photo of the face of Tom Cruise.” with hair length and age measures sampled from a final CMA-MAEGA archive for the LSI (StyleGAN2) domain. See Appendix I for more detail.

We include runs for MAP-Elites and MAP-Elites (line) on the LSI (StyleGAN2) domain in Table 1 for comparison purposes. In the LSI (StyleGAN2) domain, the two algorithms drift out of distribution and suffer a regularization penalty that results in negative objective values. We observe that the gap in performance between derivative-free QD algorithms and DQD algorithms is higher in the LSI (StyleGAN2) domain than in LSI (StyleGAN) domain. This highlights the benefits of leveraging gradients of the objective and measure functions in high-dimensional search spaces.

7 ON THE ROBUSTNESS OF CMA-MAE

Next, we present two studies that evaluate CMA-MAE robustness across two hyperparameters that may affect algorithm performance: the archive learning rate α and the archive resolution.

Archive Learning Rate. We examine the effect of different archive learning rates on the performance of CMA-MAE in the linear projection and arm repertoire domains. We vary the learning rate from 0 to 1 on an exponential scale, while keeping the resolution constant.

Table 3 shows that running CMA-MAE with the different $0 < \alpha < 1$ values results in similar performance, showing that CMA-MAE is fairly robust to the exact choice of α value. On the other hand, if $\alpha = 0$ or $\alpha = 1$ the performance drops drastically. Setting $\alpha = 1$ results in very similar performance with CMA-ME, which supports our insight from Theorem 5.2.

Archive Resolution. As noted in prior work [14, 21], quality diversity algorithms in the MAP-Elites family sometimes perform differently when run with different archive resolutions. For example, in the linear projection domain proposed in prior work [26], CMA-ME outperformed MAP-Elites and MAP-Elites (line) for archives of resolution 500×500 , while in this paper we observe that it performs worse for resolution 100×100 . In this study, we investigate how CMA-MAE performs at different archive resolutions.

First, we note that the optimal archive learning rate α is dependent on the resolution of the archive. Consider as an example a sequence of solution additions to two archives A_1 and A_2 of resolution 100×100 and 200×200 , respectively. A_2 subdivides each cell in A_1 into four cells, thus archive A_2 ’s thresholds t_e should increase at a four times faster rate than A_1 . To account for this difference, we compute α_2 for A_2 via a conversion formula $\alpha_2 = 1 - (1 - \alpha_1)^r$ (see derivation in Appendix G), where r is the ratio of cell counts between archives A_1 and A_2 . We initialize $\alpha_1 = 0.01$ for A_1 . In the above example, $\alpha_2 = 1 - (1 - 0.01)^4 = 0.0394$.

Fig. 5 shows the QD-score of CMA-MAE with the resolution-dependent archive learning rate and the baselines for each benchmark domain. CMA-ME performs worse as the resolution decreases because the archive changes quickly at small resolutions, affecting CMA-ME’s adaptation mechanism. On the contrary, MAP-Elites and MAP-Elites (line) perform worse as the resolution increases

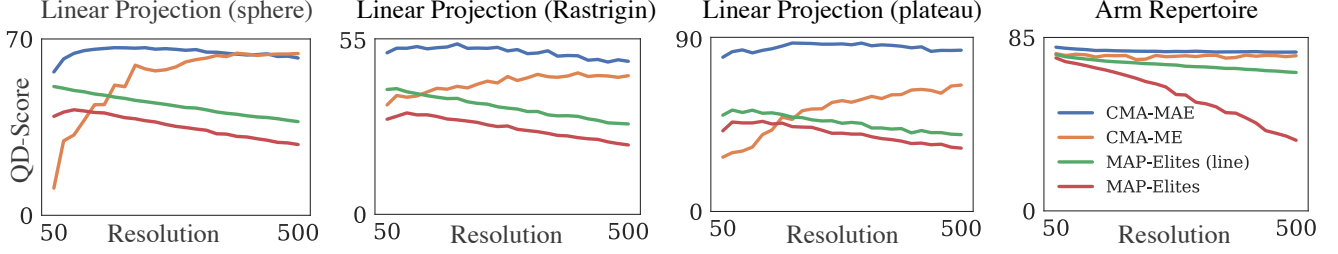


Figure 5: Final QD-score of each algorithm for 25 different archive resolutions.

	LP (sphere)		LP (Rastrigin)		LP (plateau)		Arm Repertoire	
α (CMA-MAE)	QD-score	Coverage	QD-score	Coverage	QD-score	Coverage	QD-score	Coverage
0.000	5.82	6.06%	5.33	6.24%	19.49	19.49%	65.91	66.25%
0.001	62.65	79.36%	47.87	68.10%	77.60	77.68%	78.63	79.07%
0.010	64.86	83.31%	52.65	80.56%	79.27	79.29%	79.03	79.24%
0.100	60.42	76.19%	48.74	72.50%	83.21	83.21%	78.74	78.85%
1.000	37.01	43.50%	37.86	52.82%	34.00	34.00%	75.94	76.01%

Table 3: Mean QD metrics after 10,000 iterations for CMA-MAE at different learning rates.

due to having more elites to perturb. CMA-MAE’s performance is invariant to the resolution of the archive.

8 RELATED WORK

Quality Diversity Optimization. The predecessor to quality diversity optimization, simply called diversity optimization, originated with the Novelty Search algorithm [54], which searches for a collection of solutions that are diverse in measure space. Later work introduced the Novelty Search with Local Competition (NSLC) [55] and MAP-Elites [15, 59] algorithms, which combined single-objective optimization with diversity optimization and were the first QD algorithms. Since then, several QD algorithms have been proposed, based on a variety of single-objective optimization methods, such as Bayesian optimization [49], evolution strategies [10, 11, 26], differential evolution [9], and gradient ascent [21]. Several works have improved selection mechanisms [16, 71], archives [23, 72, 78], perturbation operators [61, 79], and resolution scaling [13, 23, 32].

QD with Gradient Information. Several works combine gradient information with QD optimization without leveraging the objective and measure gradients directly. For example, in model-based QD optimization [7, 28, 29, 34, 48, 57, 80], prior work [68] trains an autoencoder on the archive of solutions and leverages the Jacobian of the decoder network to compute the covariance of the Gaussian perturbation. Works in quality diversity reinforcement learning (QD-RL) [60, 63, 65, 76] approximate a reward gradient or diversity gradient via a critic network, action space noise, or evolution strategies and incorporate those gradients into a QD-RL algorithm.

Acceptance Thresholds. Our proposed archive learning rate α was loosely inspired by simulated annealing methods [2] that maintain an acceptance threshold that gradually becomes more selective as the algorithm progresses. The notion of an acceptance threshold is also closely related to minimal criterion methods in evolutionary computation [5, 6, 53, 73]. Our work differs by both 1) maintaining an acceptance threshold per archive cell rather than a global threshold and 2) annealing the threshold.

9 LIMITATIONS AND FUTURE WORK

Our approach introduced two hyperparameters, α and \min_f (see Appendix J for \min_f analysis), to control the rate that $f - f_A$ changes. We observed that an α set strictly between 0 and 1 yields theoretical exploration improvements and that CMA-MAE is robust with respect to the exact choice of α . We additionally derived a conversion formula that converts an α_1 for a specific archive resolution to an equivalent α_2 for a different resolution. However, the conversion formula still requires practitioners to specify a good initial value of α_1 . Future work will explore ways to automatically initialize α , similar to how CMA-ES automatically assigns internal parameters [35].

CMA-MAE’s DQD counterpart CMA-MAEGA sets a new state-of-the-art in DQD optimization. However, observing its performance benefits required the more challenging LSI (StyleGAN2) domain. This highlights the need for more challenging DQD problems to advance research in DQD algorithms, since many of the current benchmark domains can be solved optimally by existing algorithms.

Quality diversity optimization is a rapidly growing branch of stochastic optimization with applications in generative design [28, 29, 33], automatic scenario generation in robotics [20, 22, 25], reinforcement learning [60, 63, 65, 76], damage recovery in robotics [15], and procedural content generation [4, 17, 24, 31, 50, 69, 70, 75, 80]. Our paper introduces a new quality diversity algorithm, CMA-MAE. Our theoretical findings inform our experiments, which show that CMA-MAE addresses three major limitations affecting CMA-ME, leading to state-of-the-art performance and robustness.

10 ACKNOWLEDGMENTS

This work was supported by the NSF CAREER Award (#2145077) and NSF NRI (#2024949). We thank Bryon Tjanaka and David Lee for their helpful discussions and feedback when deriving the batch threshold update rule in Appendix H. We would also like to thank Lisa B. Soros for her feedback on a preliminary version of this paper.

REFERENCES

- [1] AKIMOTO, Y., NAGATA, Y., ONO, I., AND KOBAYASHI, S. Bidirectional relation between cma evolution strategies and natural evolution strategies. In *International Conference on Parallel Problem Solving from Nature* (2010), Springer, pp. 154–163.
- [2] BERTSIMAS, D., AND TSITSIKLIS, J. Simulated annealing. *Statistical science* 8, 1 (1993), 10–15.
- [3] BESNIER, V., JAIN, H., BURSUC, A., CORD, M., AND PÉREZ, P. This dataset does not exist: training models from generated images. In *ICASSP 2020-2020 IEEE International Conference on Acoustics, Speech and Signal Processing (ICASSP)* (2020), IEEE, pp. 1–5.
- [4] BHATT, V., TJANAKA, B., FONTAINE, M., AND NIKOLAIDIS, S. Deep surrogate assisted generation of environments. *Advances in Neural Information Processing Systems* (2022).
- [5] BRANT, J. C., AND STANLEY, K. O. Minimal criterion coevolution: a new approach to open-ended search. In *Proceedings of the Genetic and Evolutionary Computation Conference* (2017), pp. 67–74.
- [6] BRANT, J. C., AND STANLEY, K. O. Diversity preservation in minimal criterion coevolution through resource limitation. In *Proceedings of the 2020 Genetic and Evolutionary Computation Conference* (2020), pp. 58–66.
- [7] CAZENILLE, L., BREDECHE, N., AND AUBERT-KATO, N. Exploring self-assembling behaviors in a swarm of bio-micro-robots using surrogate-assisted map-elites-elites. In *2019 IEEE Symposium Series on Computational Intelligence (SSCI)* (2019), IEEE, pp. 238–246.
- [8] CHATZILYGEROUDIS, K., CULLY, A., VASSILIADES, V., AND MOURET, J.-B. Quality-diversity optimization: a novel branch of stochastic optimization. In *Black Box Optimization, Machine Learning, and No-Free Lunch Theorems*. Springer, 2021, pp. 109–135.
- [9] CHOI, T. J., AND TOGELIUS, J. *Self-Referential Quality Diversity through Differential MAP-Elites*. Association for Computing Machinery, New York, NY, USA, 2021, p. 502–509.
- [10] COLAS, C., MADHAVAN, V., HUIZINGA, J., AND CLUNE, J. Scaling map-elites to deep neuroevolution. In *Proceedings of the 2020 Genetic and Evolutionary Computation Conference* (2020), pp. 67–75.
- [11] CONTI, E., MADHAVAN, V., PETROSKI SUCH, F., LEHMAN, J., STANLEY, K., AND CLUNE, J. Improving exploration in evolution strategies for deep reinforcement learning via a population of novelty-seeking agents. *Advances in neural information processing systems* 31 (2018).
- [12] CROWSON, K., BIDERMAN, S., KORNIS, D., STANDER, D., HALLAHAN, E., CASTRICATO, L., AND RAFF, E. Vqgan-clip: Open domain image generation and editing with natural language guidance. *arXiv preprint arXiv:2204.08583* (2022).
- [13] CULLY, A. Autonomous skill discovery with quality-diversity and unsupervised descriptors. In *Proceedings of the Genetic and Evolutionary Computation Conference* (2019), pp. 81–89.
- [14] CULLY, A. Multi-emitter map-elites: improving quality, diversity and data efficiency with heterogeneous sets of emitters. In *Proceedings of the Genetic and Evolutionary Computation Conference* (2021), pp. 84–92.
- [15] CULLY, A., CLUNE, J., TARAPORE, D., AND MOURET, J.-B. Robots that can adapt like animals. *Nature* 521, 7553 (2015), 503.
- [16] CULLY, A., AND DEMIRIS, Y. Quality and diversity optimization: A unifying modular framework. *IEEE Transactions on Evolutionary Computation* 22, 2 (2017), 245–259.
- [17] EARLE, S., SNIDER, J., FONTAINE, M. C., NIKOLAIDIS, S., AND TOGELIUS, J. Illuminating diverse neural cellular automata for level generation. *arXiv preprint arXiv:2109.05489* (2021).
- [18] ECOFFET, A., CLUNE, J., AND LEHMAN, J. Open questions in creating safe open-ended ai: tensions between control and creativity. *arXiv preprint arXiv:2006.07495* (2020).
- [19] FEFFERMAN, C., MITTER, S., AND NARAYANAN, H. Testing the manifold hypothesis. *Journal of the American Mathematical Society* 29, 4 (2016), 983–1049.
- [20] FONTAINE, M., HSU, S., ZHANG, Y., TJANAKA, B., AND NIKOLAIDIS, S. On the importance of environments in human-robot coordination. *Robotics: Science and Systems (RSS)* (2021).
- [21] FONTAINE, M., AND NIKOLAIDIS, S. Differentiable quality diversity. *Advances in Neural Information Processing Systems* 34 (2021).
- [22] FONTAINE, M., AND NIKOLAIDIS, S. A quality diversity approach to automatically generating human-robot interaction scenarios in shared autonomy. *Robotics: Science and Systems* (2021).
- [23] FONTAINE, M. C., LEE, S., SOROS, L. B., DE MESENTIER SILVA, F., TOGELIUS, J., AND HOOVER, A. K. Mapping hearthstone deck spaces through map-elites with sliding boundaries. In *Proceedings of The Genetic and Evolutionary Computation Conference* (2019), pp. 161–169.
- [24] FONTAINE, M. C., LIU, R., TOGELIUS, J., HOOVER, A. K., AND NIKOLAIDIS, S. Illuminating mario scenes in the latent space of a generative adversarial network. In *Proceedings of the AAAI Conference on Artificial Intelligence* (2021).
- [25] FONTAINE, M. C., AND NIKOLAIDIS, S. Evaluating human-robot interaction algorithms in shared autonomy via quality diversity scenario generation. *International Journal of Human-Robot Interaction* (jul 2021).
- [26] FONTAINE, M. C., TOGELIUS, J., NIKOLAIDIS, S., AND HOOVER, A. K. Covariance matrix adaptation for the rapid illumination of behavior space. In *Proceedings of the 2020 genetic and evolutionary computation conference* (2020), pp. 94–102.
- [27] FRANS, K., SOROS, L., AND WITKOWSKI, O. Clipdraw: Exploring text-to-drawing synthesis through language-image encoders. *arXiv preprint arXiv:2106.14843* (2021).
- [28] GAIER, A., ASTEROTH, A., AND MOURET, J.-B. Data-efficient design exploration through surrogate-assisted illumination. *Evolutionary computation* 26, 3 (2018), 381–410.
- [29] GAIER, A., ASTEROTH, A., AND MOURET, J.-B. Discovering representations for black-box optimization. In *Proceedings of the 2020 Genetic and Evolutionary Computation Conference* (New York, NY, USA, 2020), GECCO '20, Association for Computing Machinery, p. 103–111.
- [30] GRAHAM, R. L., KNUTH, D. E., PATASHNIK, O., AND LIU, S. Concrete mathematics: a foundation for computer science. *Computers in Physics* 3, 5 (1989), 106–107.
- [31] GRAVINA, D., KHALIFA, A., LIAPIS, A., TOGELIUS, J., AND YANNAKAKIS, G. N. Procedural content generation through quality diversity. In *2019 IEEE Conference on Games (CoG)* (2019), IEEE, pp. 1–8.
- [32] GRILLOTTI, L., AND CULLY, A. Relevance-guided unsupervised discovery of abilities with quality-diversity algorithms. In *Proceedings of the Genetic and Evolutionary Computation Conference* (2022), pp. 77–85.
- [33] HAGG, A., BERNIS, S., ASTEROTH, A., COLTON, S., AND BÄCK, T. Expressivity of parameterized and data-driven representations in quality diversity search. In *Proceedings of the Genetic and Evolutionary Computation Conference* (New York, NY, USA, 2021), GECCO '21, Association for Computing Machinery, p. 678–686.
- [34] HAGG, A., WILDE, D., ASTEROTH, A., AND BÄCK, T. Designing air flow with surrogate-assisted phenotypic niching. In *International Conference on Parallel Problem Solving from Nature* (2020), Springer, pp. 140–153.
- [35] HANSEN, N. The cma evolution strategy: A tutorial. *arXiv preprint arXiv:1604.00772* (2016).
- [36] HANSEN, N., AUGER, A., MERSMANN, O., TUSAR, T., AND BROCKHOFF, D. Coco: A platform for comparing continuous optimizers in a black-box setting.
- [37] HANSEN, N., AUGER, A., ROS, R., FINCK, S., AND POŠÍK, P. Comparing results of 31 algorithms from the black-box optimization benchmarking bbob-2009. pp. 1689–1696.
- [38] HANSEN, N., MÜLLER, S. D., AND KOUMOUTSAKOS, P. Reducing the time complexity of the derandomized evolution strategy with covariance matrix adaptation (cma-es). *Evolutionary computation* 11, 1 (2003), 1–18.
- [39] HANSEN, N., AND OSTERMEIER, A. Convergence properties of evolution strategies with the derandomized covariance matrix adaptation: The (μ)-es. *Eufit* 97 (1997), 650–654.
- [40] HENDRYCKS, D., CARLINI, N., SCHULMAN, J., AND STEINHARDT, J. Unsolved problems in ml safety. *arXiv preprint arXiv:2109.13916* (2021).
- [41] JAHANIAN, A., PUIG, X., TIAN, Y., AND ISOLA, P. Generative models as a data source for multiview representation learning. *arXiv preprint arXiv:2106.05258* (2021).
- [42] JAIN, N., OLMO, A., SENGUPTA, S., MANIKONDA, L., AND KAMBHAMPATI, S. Imperfect imagination: Implications of gans exacerbating biases on facial data augmentation and snapchat selfie lenses. *arXiv preprint arXiv:2001.09528* (2020).
- [43] JOHNSON, N. L., KOTZ, S., AND BALAKRISHNAN, N. *Continuous univariate distributions, volume 2*, vol. 289. John Wiley & sons, 1995.
- [44] KARRAS, T., AITTALA, M., HELLSTEN, J., LAINE, S., LEHTINEN, J., AND AILA, T. Training generative adversarial networks with limited data. In *Proc. NeurIPS* (2020).
- [45] KARRAS, T., AITTALA, M., LAINE, S., HÄRKÖNEN, E., HELLSTEN, J., LEHTINEN, J., AND AILA, T. Alias-free generative adversarial networks. In *Proc. NeurIPS* (2021).
- [46] KARRAS, T., LAINE, S., AND AILA, T. A style-based generator architecture for generative adversarial networks. In *Proceedings of the IEEE/CVF Conference on Computer Vision and Pattern Recognition* (2019), pp. 4401–4410.
- [47] KARRAS, T., LAINE, S., AITTALA, M., HELLSTEN, J., LEHTINEN, J., AND AILA, T. Analyzing and improving the image quality of stylegan. In *Proceedings of the IEEE/CVF Conference on Computer Vision and Pattern Recognition (CVPR)* (June 2020).
- [48] KELLER, L., TANNEBERG, D., STARK, S., AND PETERS, J. Model-based quality-diversity search for efficient robot learning. *2020 IEEE/RSJ International Conference on Intelligent Robots and Systems (IROS)* (2020), 9675–9680.
- [49] KENT, P., AND BRANKE, J. Bop-elites, a bayesian optimisation algorithm for quality-diversity search. *arXiv preprint arXiv:2005.04320* (2020).
- [50] KHALIFA, A., LEE, S., NEALEN, A., AND TOGELIUS, J. Talakat: Bullet hell generation through constrained map-elites. In *Proceedings of The Genetic and Evolutionary Computation Conference* (2018), pp. 1047–1054.
- [51] KINGMA, D. P., AND BA, J. Adam: A method for stochastic optimization. In *3rd*

- International Conference on Learning Representations, ICLR 2015, San Diego, CA, USA, May 7-9, 2015, Conference Track Proceedings* (2015).
- [52] LEHMAN, J., CLUNE, J., MISEVIC, D., ADAMI, C., ALTENBERG, L., BEAULIEU, J., BENTLEY, P. J., BERNARD, S., BESLON, G., BRYSON, D. M., ET AL. The surprising creativity of digital evolution: A collection of anecdotes from the evolutionary computation and artificial life research communities. *Artificial life* 26, 2 (2020), 274–306.
 - [53] LEHMAN, J., AND STANLEY, K. O. Revising the evolutionary computation abstraction: minimal criteria novelty search. In *Proceedings of the 12th annual conference on Genetic and evolutionary computation* (2010), pp. 103–110.
 - [54] LEHMAN, J., AND STANLEY, K. O. Abandoning objectives: Evolution through the search for novelty alone. *Evolutionary computation* 19, 2 (2011), 189–223.
 - [55] LEHMAN, J., AND STANLEY, K. O. Evolving a diversity of virtual creatures through novelty search and local competition. In *Proceedings of the 13th annual conference on Genetic and evolutionary computation* (2011), pp. 211–218.
 - [56] LIM, B., ALLARD, M., GRILLOTTI, L., AND CULLY, A. Accelerated quality-diversity for robotics through massive parallelism. In *ICLR Workshop on Agent Learning in Open-Endedness* (2022).
 - [57] LIM, B., GRILLOTTI, L., BERNASCONI, L., AND CULLY, A. Dynamics-aware quality-diversity for efficient learning of skill repertoires. *ArXiv abs/2109.08522* (2021).
 - [58] MENON, S., DAMIAN, A., HU, S., RAVI, N., AND RUDIN, C. Pulse: Self-supervised photo upsampling via latent space exploration of generative models. In *Proceedings of the IEEE/CVF Conference on Computer Vision and Pattern Recognition* (2020), pp. 2437–2445.
 - [59] MOURET, J.-B., AND CLUNE, J. Illuminating search spaces by mapping elites. *arXiv preprint arXiv:1504.04909* (2015).
 - [60] NILSSON, O., AND CULLY, A. Policy gradient assisted map-elites. *Proceedings of the Genetic and Evolutionary Computation Conference* (2021).
 - [61] NORDMOEN, J., SAMUELSEN, E., ELLEFSEN, K. O., AND GLETTE, K. Dynamic mutation in map-elites for robotic repertoire generation. In *Artificial Life Conference Proceedings* (2018), MIT Press, pp. 598–605.
 - [62] PAOLO, G., CONINX, A., DONCIEUX, S., AND LAFLAQUIÈRE, A. Sparse reward exploration via novelty search and emitters. In *Proceedings of the Genetic and Evolutionary Computation Conference* (2021), pp. 154–162.
 - [63] PARKER-HOLDER, J., PACCHIANO, A., CHOROMANSKI, K. M., AND ROBERTS, S. J. Effective diversity in population based reinforcement learning. In *Advances in Neural Information Processing Systems* (2020), H. Larochelle, M. Ranzato, R. Hadsell, M. F. Balcan, and H. Lin, Eds., vol. 33, Curran Associates, Inc., pp. 18050–18062.
 - [64] PEREZ, V. Generating images from prompts using clip and stylegan, 2021. MIT License.
 - [65] PIERROT, T., MACÉ, V., CIDERON, G., BEGUIR, K., CULLY, A., SIGAUD, O., AND PERRIN-GILBERT, N. Diversity policy gradient for sample efficient quality-diversity optimization. *arXiv e-prints* (2020), arXiv:2006.
 - [66] PUGH, J. K., SOROS, L. B., SZERLIP, P. A., AND STANLEY, K. O. Confronting the challenge of quality diversity. In *Proceedings of the 2015 Annual Conference on Genetic and Evolutionary Computation* (2015), pp. 967–974.
 - [67] RADFORD, A., KIM, J. W., HALLACY, C., RAMESH, A., GOH, G., AGARWAL, S., SASTRY, G., ASKELL, A., MISHKIN, P., CLARK, J., KRUEGER, G., AND SUTSKEVER, I. Learning transferable visual models from natural language supervision. In *Proceedings of the 38th International Conference on Machine Learning ICML 2021* (2021).
 - [68] RAKICEVIC, N., CULLY, A., AND KORMUSHEV, P. Policy manifold search: Exploring the manifold hypothesis for diversity-based neuroevolution. In *Proceedings of the Genetic and Evolutionary Computation Conference* (New York, NY, USA, 2021), GECCO '21, Association for Computing Machinery, p. 901–909.
 - [69] SARKAR, A., AND COOPER, S. Generating and blending game levels via quality-diversity in the latent space of a variational autoencoder. *arXiv preprint arXiv:2102.12463* (2021).
 - [70] SCHRUM, J., VOLZ, V., AND RISI, S. Cppn2gan: Combining compositional pattern producing networks and gans for large-scale pattern generation. In *Proceedings of the 2020 Genetic and Evolutionary Computation Conference* (2020), pp. 139–147.
 - [71] SFIKAS, K., LIAPIS, A., AND YANNAKAKIS, G. N. Monte carlo elites: Quality-diversity selection as a multi-armed bandit problem. In *Proceedings of the Genetic and Evolutionary Computation Conference* (New York, NY, USA, 2021), GECCO '21, Association for Computing Machinery, p. 180–188.
 - [72] SMITH, D., TOKARCHUK, L., AND WIGGINS, G. Rapid phenotypic landscape exploration through hierarchical spatial partitioning. In *International conference on parallel problem solving from nature* (2016), Springer, pp. 911–920.
 - [73] STANLEY, K. O., CHENEY, N., AND SOROS, L. How the strictness of the minimal criterion impacts open-ended evolution. In *ALIFE 2016, the Fifteenth International Conference on the Synthesis and Simulation of Living Systems* (2016), MIT Press, pp. 208–215.
 - [74] STANLEY, K. O., LEHMAN, J., AND SOROS, L. Open-endedness: The last grand challenge you've never heard of. *While open-endedness could be a force for discovering intelligence, it could also be a component of AI itself* (2017).
 - [75] STECKEL, K., AND SCHRUM, J. Illuminating the space of beatable lode runner levels produced by various generative adversarial networks. In *Proceedings of the Genetic and Evolutionary Computation Conference Companion* (New York, NY, USA, 2021), GECCO '21, Association for Computing Machinery, p. 111–112.
 - [76] TJANAKA, B., FONTAINE, M. C., TOGELIUS, J., AND NIKOLAIDIS, S. Approximating gradients for differentiable quality diversity in reinforcement learning. *GECCO* (2022).
 - [77] TJANAKA, B., FONTAINE, M. C., ZHANG, Y., SOMMERER, S., DENNLER, N., AND NIKOLAIDIS, S. pyribs: A bare-bones python library for quality diversity optimization. <https://github.com/icaros-usc/pyribs>, 2021.
 - [78] VASSILIADES, V., CHATZILYGEROUDIS, K., AND MOURET, J.-B. Using centroidal voronoi tessellations to scale up the multidimensional archive of phenotypic elites algorithm. *IEEE Transactions on Evolutionary Computation* 22, 4 (2018), 623–630.
 - [79] VASSILIADES, V., AND MOURET, J.-B. Discovering the elite hypervolume by leveraging interspecies correlation. In *Proceedings of the Genetic and Evolutionary Computation Conference* (2018), pp. 149–156.
 - [80] ZHANG, Y., FONTAINE, M. C., HOOVER, A. K., AND NIKOLAIDIS, S. Deep surrogate assisted map-elites for automated hearthstone deckbuilding. *arXiv preprint arXiv:2112.03534* (2021).

APPENDIX

A HYPERPARAMETER SELECTION

For all domains we mirror the hyperparameter selection of prior work [21]. For CMA-MAE and CMA-MAEGA, we duplicate the hyperparameter selections of CMA-ME and CMA-MEGA, respectively. Following prior work [26], we run all algorithms with 15 emitters on the linear projection and arm repertoire domains. In the latent space illumination domain, we run experiments with only one emitter, due to the computational expense of the domain. Emitters are independent CMA-ES instances that run in parallel with a shared archive. For each algorithm, we select a batch size $\lambda = 36$ following prior work [21]. For MAP-Elites and MAP-Elites (line), we initialize the archive with 100 random solutions, sampled from the distribution $\mathcal{N}(\mathbf{0}, I)$. These initial solutions do not count in the evaluation budget for MAP-Elites and MAP-Elites (line). For algorithms in the CMA-ME family (CMA-ME, CMA-MAE, CMA-MEGA, and CMA-MAEGA), we initialize $\theta_0 = \mathbf{0}$ for every domain.

In our experiments we want to directly compare the ranking mechanisms of CMA-ME and CMA-MAE. However, CMA-ME is typically run with a “no improvement” restart rule, where the algorithm will restart if no solution changes the archive. Due to CMA-MAE’s annealed acceptance threshold t_e , a “no improvement” restart rule would cause CMA-ME and CMA-MAE to restart at different rates, confounding the effects of restarts and rankings. Filter selection also has a similar confounding effect as solutions are selected if they change the archive. For these reasons, in the main paper we run CMA-ME with a basic restart rule (CMA-ES style restarts only [35]) and μ selection [35] (selecting the top half of the ranking). In Appendix Section L, we run an extra CMA-ME with filter selection and the “no improvement” restart rule, which we denote CMA-ME*. We include, as an additional baseline, a configuration of CMA-ME that mixes emitters that optimize only for the objective with emitters that optimize for improvement, a configuration first studied in prior work [14]. We refer to this configuration as CMA-ME (imp, opt).

In the latent space illumination domain, due to the computational expense of the domain, we compare directly against the results in prior work [21], where we obtained the data (MIT license) with consent from the authors. For CMA-MAE and CMA-MAEGA we include the “no improvement” restart rule to match CMA-ME and CMA-MEGA as closely as possible. For this domain, we take gradient steps with the Adam optimizer [51], following the recommendation of prior work [21]. However, we run CMA-MAE with μ selection, since we found that small values of the archive learning rate α make filter selection worse.

In Appendix I, we describe a second LSI experiment on StyleGAN2 [47] configured by insights from the generative art community that improve the quality of single-objective latent space optimization. For this domain, we configure CMA-MAEGA and CMA-MEGA to use a “basic” restart rule because the latent space L2 regularization keeps solutions in the StyleGAN2 training distribution. For this experiment, the latent space is large ($n = 9216$), so we exclude CMA-ME and CMA-MAE due to the size of the covariance matrix (9216×9216) and the prohibitive cost for computing an eigendecomposition of a large covariance matrix.

Linear Projection (sphere, Rastrigin, plateau).

- MAP-Elites: $\sigma = 0.5$
- MAP-Elites (line): $\sigma_1 = 0.5, \sigma_2 = 0.2$
- CMA-ME: $\sigma = 0.5, \mu$ selection, basic restart rule
- CMA-ME*: $\sigma = 0.5$, filter selection, no improvement restart rule
- CMA-ME (imp, opt): $\sigma = 0.5, \mu$ selection, basic restart rule, 7 optimizing and 8 improvement emitters
- CMA-MAE: $\sigma = 0.5, \alpha = 0.01, \min_f = 0, \mu$ selection, basic restart rule
- CMA-MEGA: $\sigma_g = 10.0, \eta = 1.0$, basic restart rule, gradient ascent optimizer
- CMA-MAEGA: $\sigma_g = 10.0, \eta = 1.0, \alpha = 0.01, \min_f = 0$, basic restart rule, gradient ascent optimizer

Arm Repertoire.

- MAP-Elites: $\sigma = 0.1$
- MAP-Elites (line): $\sigma_1 = 0.1, \sigma_2 = 0.2$
- CMA-ME: $\sigma = 0.2, \mu$ selection, basic restart rule
- CMA-ME*: $\sigma = 0.2$, filter selection, no improvement restart rule
- CMA-ME (imp, opt): $\sigma = 0.2, \mu$ selection, basic restart rule, 7 optimizing and 8 improvement emitters
- CMA-MAE: $\sigma = 0.2, \alpha = 0.01, \min_f = 0, \mu$ selection, basic restart rule
- CMA-MEGA: $\sigma_g = 0.05, \eta = 1.0$, basic restart rule, gradient ascent optimizer
- CMA-MAEGA: $\sigma_g = 0.05, \eta = 1.0, \alpha = 0.01, \min_f = 0$, basic restart rule, gradient ascent optimizer

Latent Space Illumination. (StyleGAN)

- MAP-Elites: $\sigma = 0.2$
- MAP-Elites (line): $\sigma_1 = 0.1, \sigma_2 = 0.2$
- CMA-ME: $\sigma = 0.02$, filter selection, no improvement restart rule
- CMA-MAE: $\sigma = 0.02, \alpha = 0.1, \min_f = 55, \mu$ selection, no improvement restart rule, 50 iteration timeout

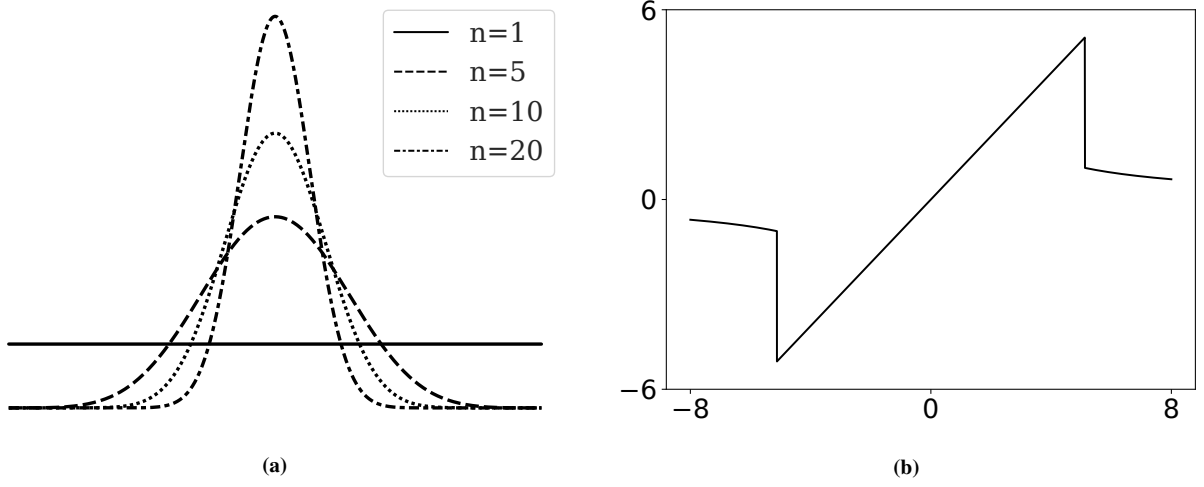


Figure 6: Measure function figures reproduced from prior work [21, 26] with the authors’ permission. (a) a Bates distribution. (b) clip function for defining the measures in the linear projection domain.

- CMA-MEGA: $\sigma_g = 0.002$, $\eta = 0.002$, Adam optimizer, no improvement restart rule
- CMA-MAEGA: $\sigma_g = 0.002$, $\eta = 0.002$, $\alpha = 0.1$, $\min_f = 55$, Adam optimizer, no improvement restart rule, 50 iteration timeout

Latent Space Illumination. (StyleGAN 2)

- MAP-Elites: $\sigma = 0.1$
- MAP-Elites (line): $\sigma_1 = 0.1$, $\sigma_2 = 0.2$
- CMA-MEGA: $\sigma_g = 0.01$, $\eta = 0.05$, Adam optimizer, basic restart rule
- CMA-MAEGA: $\sigma_g = 0.01$, $\eta = 0.05$, $\alpha = 0.02$, $\min_f = 0$, Adam optimizer, basic restart rule

Adam Hyperparameters. We use the same hyperparameters as previous work [21, 64].

- $\beta_1 = 0.9$
- $\beta_2 = 0.999$

Archives. For the linear projection and arm repertoire domains, we initialize an archive of 100×100 cells for all algorithms. For latent space illumination we initialize an archive of 200×200 cells for all algorithms, following prior work [21].

B DOMAIN DETAILS

To experimentally evaluate both CMA-MAE and CMA-MAEGA, we select domains from prior work on DQD [21]: linear projection [26], arm repertoire [16], and latent space illumination [24]. While many quality diversity optimization domains exist, we select these because gradients of f and \mathbf{m} are easy to compute analytically and allow us to evaluate DQD algorithms in addition to derivative-free QD algorithms. To evaluate the good exploration properties of CMA-MAE on flat objectives, we introduce a variant of the linear projection domain to include a “plateau” objective function.

Linear Projection. The linear projection domain [26] was introduced to benchmark distortions caused by mapping a high-dimensional search space to a low-dimensional measure space. The domain forms a 2D measure space by a linear projection that bounds the contribution of each component θ_i of the projection to the range $[-5.12, 5.12]$. QD algorithms must adapt the step size of each component θ_i to slowly approach the extremes of the measure space, with a harsh penalty for components outside $[-5.12, 5.12]$. As QD domains must provide an objective, the linear projection domain included two objectives from the black-box optimization benchmarks [36, 37]: sphere and Rastrigin. Following prior work [26], we run all experiments for $n = 100$.

Formally, the measure functions are defined as a linear projection, a weighted sum of the components $\theta_i \in \mathbb{R}$ of a solution $\theta \in \mathbb{R}^n$. The first measure function m_1 is a weighted sum of the first half of the solution θ , and the second measure function m_2 is a weighted sum of the second half of the solution θ (see Eq. 3). To ensure that all solutions mapped to measure space occupy a finite volume, the contribution in measure space of each component θ_i is bounded to the range $[-5.12, 5.12]$ via a clip function (see Eq. 2) that applies a harsh penalty for solution components θ_i stepping outside the range $[-5.12, 5.12]$.

$$\text{clip}(\theta_i) = \begin{cases} \theta_i & \text{if } -5.12 \leq \theta_i \leq 5.12 \\ 5.12/\theta_i & \text{otherwise} \end{cases} \quad (2)$$

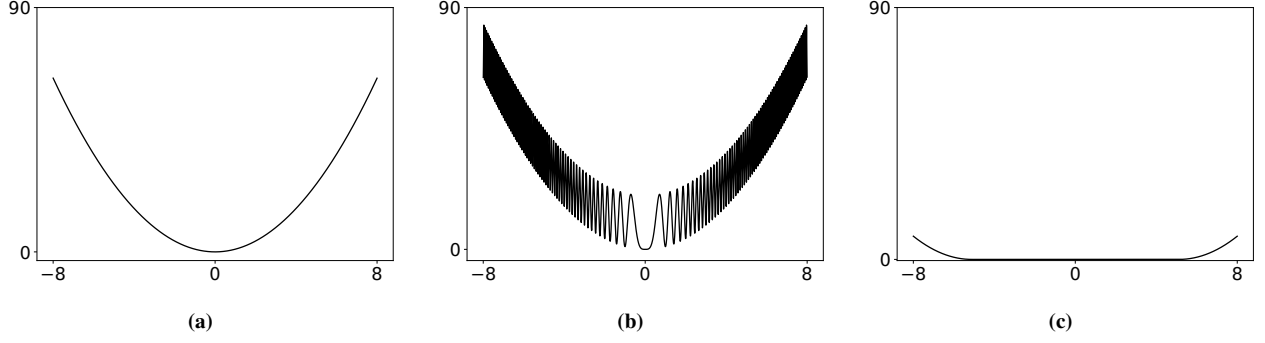


Figure 7: Objective functions for the linear projection domain in their minimization form for $n = 1$. (a) a sphere function. (b) the Rastrigin function. (c) a plateau function.

$$m(\theta) = \left(\sum_{i=1}^{\lfloor \frac{n}{2} \rfloor} \text{clip}(\theta_i), \sum_{i=\lfloor \frac{n}{2} \rfloor + 1}^n \text{clip}(\theta_i) \right) \quad (3)$$

Fig. 6 visualizes *why* the linear projection domain is challenging. First, we note that the density of solutions in search space mapped to measure space mostly occupies the region close to $\mathbf{0}$. To justify why, consider sampling uniformly in the hypercube $[-5.12, 5.12]^n$ in search space. We note that each of these points maps to the linear region of the measure functions and each of our measures becomes a sum of random variables. If we divide by n , we normalize by the dimensions of the search space, then the measure functions become an *average* of random variables. The average of n uniform random variables is the Bates distribution [43], a distribution that narrows in variance as n grows larger. Without the *clip* function, a QD algorithm could simply increase a single θ_i to reach any point in the measure space. However, the clip function prevents this by bounding the contribution of each component of θ to the range $[-5.12, 5.12]$. To reach the extremes of measure space all components θ_i must converge to the extremums ± 5.12 . The linear projection domain is challenging to explore due to both the clustering of solutions in a small region of measure space and the heavy measure space penalties applied by the clip function when a component θ_i leaves the region $[-5.12, 5.12]$.

Next, we describe the linear projection domain’s objective functions visualized in Fig. 7.

The objectives of the linear projection domain satisfy the requirements that a QD domain needs to have an objective and are of lesser importance than the measure function definitions, since the benchmark primarily evaluates exploration capabilities. Prior work [26] selected two objectives from the black-box optimization benchmarks competition [36, 37]: sphere and Rastrigin. The sphere function (Eq. 4) is a quadratic function³, while the Rastrigin function (Eq. 5) is a multi-modal function that when smoothed is quadratic. The domain shifts the global optimum to the position $\theta_i = 5.12 \cdot 0.4 = 2.048$.

$$f_{\text{sphere}}(\theta) = \sum_{i=1}^n \theta_i^2 \quad (4)$$

$$f_{\text{Rastrigin}}(\theta) = 10n + \sum_{i=1}^n [\theta_i^2 - 10 \cos(2\pi\theta_i^2)] \quad (5)$$

We introduce an additional objective to evaluate the good exploration properties of CMA-MAE on flat objectives. Our “plateau” objective function (Eq. 7) is constant everywhere, but with a quadratic penalty for each component outside the range $[-5.12, 5.12]$. The penalty acts as a regularizer to encourage algorithms to search in the linear region of measure space.

$$f_{\text{plateau}}(\theta_i) = \begin{cases} 0 & \text{if } -5.12 \leq \theta_i \leq 5.12 \\ (|\theta_i| - 5.12)^2 & \text{otherwise} \end{cases} \quad (6)$$

$$f_{\text{plateau}}(\theta) = \frac{1}{n} \sum_{i=1}^n f_{\text{plateau}}(\theta_i) \quad (7)$$

Arm Repertoire. The arm repertoire domain [16, 79] tasks QD algorithms to find a diverse collection of arm positions for an n -dimensional planar robotic arm with revolute joints. The measures in this domain are the 2D coordinates of the robot’s end-effector and the objective is to minimize the variance of the joint angles.

³In derivative-free optimization many of the benchmark functions are named after the shape of the contour lines. In the case of quadratic functions with an identity Hessian matrix, the contour lines form hyperspheres.

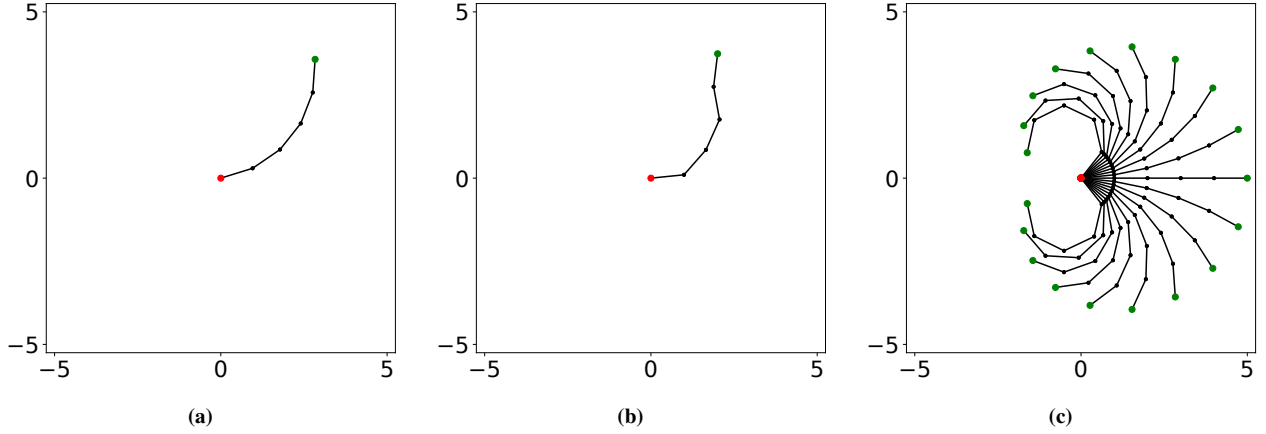


Figure 8: Examples of the Arm Repertoire domain for $n = 5$. The figures are reproduced from previous work [21] with the authors’ permission. (a) An optimal grasp with 0 variance between joint angles. (b) A sub-optimal grasp. (c) An ensemble of 0 variance optimal grasps.

In Fig. 8, we visualize example arms for $n = 5$ (5-DOF). The optimal solutions in this domain have 0 variance between all joint angles. The measure functions are bounded to the range $[-n, n]$ as each arm segment has a unit length. The reachable cells form a circle of radius n . Therefore, the optimal archive coverage is approximately $\frac{\pi n^2}{4n^2} \approx 78.5\%$. An archive can achieve an upper-bound of this ratio that becomes tighter at higher resolutions. We select $n = 100$ (100-DOF) arms for the experiments.

Latent Space Illumination. Prior work introduced the latent space illumination problem [24], the problem of searching the latent space of a generative model with a quality diversity algorithm. We evaluate on the StyleGAN+CLIP version of this problem [21], by searching the latent space of StyleGAN [46] with a QD algorithm. We form the differentiable objective and measures in this domain by specifying text prompts to the CLIP model [67] that can determine the similarity of an image and text. We specify an objective prompt of “A photo of Beyoncé”. For measures, we would like to have CLIP quantify abstract concepts like the hair length or age of the person in the photo. However, CLIP can only determine similarity of an image and a text prompt. As surrogates for age and hair length, we specify the measure prompts of “A small child” and “A woman with long blonde hair”. The objective and measure functions guide the QD algorithms towards discovering a collection of photos of Beyoncé with varying age and hair length.

For our additional LSI experiment on StyleGAN2 with setup improvements, see Appendix I.

Transformations of the Objective Function. We highlight two issues that must be addressed by transforming the objective in each domain. First, we note that the problem definition in each of our domains contains an objective f that must be minimized. In contrast, the QD problem definition specifies an objective f that must be maximized. Second, the QD-score metric, which measures the performance of QD algorithms, requires a non-negative objective function. Following prior work [21, 26], we transform the objective f via a linear transformation: $f' = af + b$. The linear transformation maps function outputs to the range $[0, 100]$.

In the linear projection domain, we estimate the largest objective value for the sphere and Rastrigin function within the region $[-5.12, 5.12]$ for each solution component θ_i . We compute $f(-5.12, \dots)$ for each objective as the maximum. The minimum of each function is 0. We calculate the linear transformation as:

$$f'(\theta) = 100 \cdot \frac{f(\theta) - f_{\max}}{f_{\min} - f_{\max}} \quad (8)$$

For our new plateau objective, all solution points within the region $[-5.12, 5.12]^n$ have objective value of 0. For this objective we set $f_{\min} = 0$ and $f_{\max} = 100$ and apply the transformation in Eq. 8.

For the arm domain we select $f_{\min} = 0$ and $f_{\max} = 1$, and in the LSI domain we select $f_{\min} = 0$ and $f_{\max} = 10$. We select these values to match prior work [21].

C IMPLEMENTATION

We replicate the implementation details of prior work [21].

Archives. For the linear projection and arm repertoire domains, we initialize an archive of 100×100 cells for all algorithms. For latent space illumination we initialize an archive of 200×200 cells for all algorithms, following prior work [21].

Metrics. We use the sum of f values of all cells in the archive, defined as the QD-score [66], as a metric for the quality and diversity of solutions. Following prior work [21], we normalize the QD-score by the total number of cells, both occupied and unoccupied, to make QD-score

invariant to the resolution of the archive. We additionally compute the coverage, defined as the number of occupied cells in the archive divided by the total number of cells.

Computational Resources. We ran all trials of the linear projection and arm repertoire domains on an AMD Ryzen Threadripper 32-core (64 threads) processor. A run of 20 trials in parallel takes about 20 minutes for the linear projection domain and 25 minutes for the arm repertoire domain. For the latent space illumination domain, we accelerate the StyleGAN+CLIP pipeline on a GeForce RTX 3090 Nvidia GPU. One trial for latent space illumination takes approximately 2 hours and 30 minutes for StyleGAN and approximately 3 hours and 30 minutes for StyleGAN2. In all domains, runtime increases when an algorithm obtains better coverage, because we iterate over the archive when QD statistics are calculated.

Software Implementation. We use the open source pyribs [77] library for all algorithms. We implemented the CMA-MAE and CMA-MAEGA algorithms using the same library.

D COVARIANCE MATRIX ADAPTATION MAP-ELITES VIA A GRADIENT ARBORESCENCE (CMA-MAEGA)

In this section, we provide information of the CMA-MEGA differentiable quality diversity (DQD) algorithm, and we derive CMA-MAE’s DQD counterpart: CMA-MAEGA.

CMA-MEGA. Covariance Matrix Adaptation MAP-Elites via Gradient Arborecence (CMA-MEGA) solves the DQD problem, where the objective f and measures m are first-order differentiable. Like CMA-ME, the algorithm maintains a solution point $\theta \in \mathbb{R}^n$ and a MAP-Elites archive. CMA-MEGA samples new solutions by perturbing the search point θ via the objective and measure gradients. However, the contribution of each gradient is balanced by gradient coefficients c : $\theta_i = \theta + c_0 \nabla f(\theta) + \sum_{j=1}^k c_j \nabla m_j(\theta)$. These coefficients are sampled from a multivariate Gaussian distribution $N(\mu, \Sigma)$ maintained by the algorithm. After sampling new candidate solutions θ_i , the solutions are ranked via the improvement ranking from CMA-ME. CMA-MEGA updates $N(\mu, \Sigma)$ via the CMA-ES update rules and the algorithm steps θ also in the direction of largest archive improvement. The authors showed that CMA-MEGA approximates a natural gradient step of the QD objective (Eq. 1), but with respect to the gradient coefficients.

CMA-MAEGA. We note that our augmentations to the CMA-ME algorithm only affects how we replace solutions in the archive and how we calculate Δ_i . Both CMA-ME and CMA-MAEGA replace solutions and calculate Δ_i identically, so we apply the same augmentations from CMA-ME to CMA-MEGA to form a new DQD algorithm, CMA-MAEGA. Algorithm 2 shows the pseudo-code for CMA-MAEGA with the differences from CMA-MEGA highlighted in yellow.

E THEORETICAL PROPERTIES OF CMA-MAE

THEOREM E.1. *The CMA-ES algorithm is equivalent to CMA-MAE when $\alpha = 0$, if CMA-ES restarts from an archive solution.*

PROOF. CMA-ES and CMA-MAE differ only on how they rank solutions. CMA-ES ranks solutions purely based on the objective f , while CMA-MAE ranks solutions by $f - t_e$, where t_e is the acceptance threshold initialized by \min_f . Thus, to show that CMA-ES is equivalent to CMA-MAE for $\alpha = 0$, we only need to show that they result in identical rankings.

In CMA-MAE, t_e is updated as follows: $t_e \leftarrow (1 - \alpha)t_e + \alpha f$. For $\alpha = 0$, $t_e = \min_f$ is invariant for the whole algorithm: $t_e \leftarrow 1t_e + 0f = t_e$. Therefore, CMA-MAE ranks solutions based on $f - \min_f$. However, comparison-based sorting is invariant to order-preserving transformations of the values being sorted [35]. Thus, CMA-ES and CMA-MAE rank solutions identically. \square

Next, we prove that CMA-ME is equivalent to CMA-MAE with the following caveats. First, we assume that CMA-ME restarts only with the CMA-ES restart rules, rather than the additional “no improvement” restart condition from prior work [26]. Second, we assume that both CMA-ME and CMA-MAE leverage μ selection rather than filtering selection.

LEMMA E.2. *During execution of the CMA-MAE algorithm with $\alpha = 1$, the threshold t_e is equal to $f(\theta_e)$ for cells that are occupied by a solution θ_e and to \min_f for all empty cells.*

PROOF. We will prove the lemma by induction. All empty cells are initialized with $t_e = \min_f$, satisfying the basis step. Then, we will show that if the statement holds after k archive updates, it will hold after a subsequent update $k + 1$.

Assume that at step k we generate a new solution θ_i mapped to a cell e . We consider two cases:

Case 1: The archive cell e is empty. Then, $f(\theta_i) > \min_f$ and both CMA-ME and CMA-MAE will place θ_i in the archive as the new cell occupant θ_e . The threshold t_e is updated as $t_e = (1 - \alpha)t_e + \alpha f(\theta_e) = 0\min_f + 1f(\theta_e) = f(\theta_e)$.

Case 2: The archive cell e contains an incumbent solution θ_e . Then, either $f(\theta_i) \leq f(\theta_e)$ or $f(\theta_i) > f(\theta_e)$. If $f(\theta_i) \leq f(\theta_e)$, then the archive does not change and the inductive step holds via the inductive hypothesis. If $f(\theta_i) > f(\theta_e)$, then θ_i becomes the new cell occupant θ_e and t_e is updated as $t_e = (1 - \alpha)t_e + \alpha f(\theta_e) = 0t_e + 1f(\theta_e) = f(\theta_e)$. \square

THEOREM E.3. *The CMA-ME algorithm is equivalent to CMA-MAE when $\alpha = 1$ and \min_f is an arbitrarily large negative number.*

PROOF. Both CMA-ME and CMA-MAE rank candidate solutions θ_i based on improvement values Δ_i . While CMA-ME and CMA-MAE compute Δ_i differently, we will show that for $\alpha = 1$, the rankings are identical for the two algorithms.

```

1 CMA-MAEGA (evaluate,  $\theta_0, N, \lambda, \eta, \sigma_g, \min_f, \alpha$ )
   input : An evaluation function evaluate that computes the objective, the measures, and the gradients of the objective and measures,
           an initial solution  $\theta_0$ , a desired number of iterations  $N$ , a branching population size  $\lambda$ , a learning rate  $\eta$ , an initial step size for
           CMA-ES  $\sigma_g$ , a minimal acceptable solution quality  $\min_f$ , and an archive learning rate  $\alpha$ .
   result : Generate  $N(\lambda + 1)$  solutions storing elites in an archive  $A$ .

2 Initialize solution parameters  $\theta$  to  $\theta_0$ , CMA-ES parameters  $\mu = 0, \Sigma = \sigma_g I$ , and  $p$ , where we let  $p$  be the CMA-ES internal
   parameters.
3 Initialize the archive  $A$  and the acceptance threshold  $t_e$  with  $\min_f$  for each cell  $e$ .
4 for  $iter \leftarrow 1$  to  $N$  do
5    $f, \nabla_f, m, \nabla_m \leftarrow \text{evaluate}(\theta)$ 
6    $\nabla_f \leftarrow \text{normalize}(\nabla_f), \nabla_m \leftarrow \text{normalize}(\nabla_m)$ 
7   if  $f > t_e$  then
8     Replace the current elite in cell  $e$  of the archive  $A$  with  $\theta_i$ 
9      $t_e \leftarrow (1 - \alpha)t_e + \alpha f$ 
10  end
11  for  $i \leftarrow 1$  to  $\lambda$  do
12     $c \sim \mathcal{N}(\mu, \Sigma)$ 
13     $\nabla_i \leftarrow c_0 \nabla_f + \sum_{j=1}^k c_j \nabla_{m_j}$ 
14     $\theta'_i \leftarrow \theta + \nabla_i$ 
15     $f', *, m', * \leftarrow \text{evaluate}(\theta'_i)$ 
16     $\Delta_i \leftarrow f' - t_e$ 
17    if  $f' > t_e$  then
18      Replace the current occupant in cell  $e$  of the archive  $A$  with  $\theta_i$ 
19       $t_e \leftarrow (1 - \alpha)t_e + \alpha f'$ 
20    end
21  end
22  rank  $\nabla_i$  by  $\Delta_i$ 
23   $\nabla_{\text{step}} \leftarrow \sum_{i=1}^{\lambda} w_i \nabla_{\text{rank}[i]}$ 
24   $\theta \leftarrow \theta + \eta \nabla_{\text{step}}$ 
25  Adapt CMA-ES parameters  $\mu, \Sigma, p$  based on improvement ranking  $\Delta_i$ 
26  if there is no change in the archive then
27    Restart CMA-ES with  $\mu = 0, \Sigma = \sigma_g I$ .
28    Set  $\theta$  to a randomly selected existing cell  $\theta_i$  from the archive
29  end
30 end

```

Algorithm 2: Covariance Matrix Adaptation MAP-Annealing via a Gradient Arborescence (CMA-MAEGA)

We assume a new candidate solution mapped to a cell e . We describe first the computation of Δ_i for CMA-ME. CMA-ME ranks solutions that discover an empty cell based on their objective value. Thus, if θ_i discovers an empty cell, $\Delta_i = f(\theta_i)$. On the other hand, if θ_i is mapped to a cell occupied by another solution θ_e , it will rank θ_i based on the improvement $\Delta_i = f(\theta_i) - f(\theta_e)$. CMA-ME performs a two-stage ranking, where it ranks all solutions that discover empty cells before solutions that improve occupied cells.

We now show the computation of Δ_i for CMA-MAE with $\alpha = 1$. If θ_i discovers an empty cell $\Delta_i = f(\theta_i) - t_e$ and by Lemma E.2 $\Delta_i = f(\theta_i) - \min_f$. If θ_i is mapped to a cell occupied by another solution θ_e , $\Delta_i = f(\theta_i) - t_e$ and by Lemma E.2 $\Delta_i = f(\theta_i) - f(\theta_e)$.

Comparing the values Δ_i between the two algorithms we observe the following: (1) If θ_i discovers an empty cell, $\Delta_i = f(\theta_i) - \min_f$ for CMA-MAE. However, \min_f is a constant and comparison-based sorting is invariant to order preserving transformations [35], thus ranking by $\Delta_i = f(\theta_i) - \min_f$ is identical to ranking by $\Delta_i = f(\theta_i)$ performed by CMA-ME. (2) If θ_i is mapped to a cell occupied by another solution θ_e , $\Delta_i = f(\theta_i) - f(\theta_e)$ for both algorithms. (3) Because \min_f is an arbitrarily large negative number $f(\theta_i) - \min_f > f(\theta_i) - f(\theta_e)$. Thus, CMA-MAE will always rank solutions that discover empty cells before solutions that are mapped to occupied cells, identically to CMA-ME. \square

We next provide theoretical insights on how the discount function f_A smoothly increases from a constant function \min_f to CMA-ME's discount function as α increases from 0 to 1. We show this for the special case of a fixed sequence of candidate solutions.

THEOREM E.4. *Let α_i and α_j be two archive learning rates for archives A_i and A_j such that $0 \leq \alpha_i < \alpha_j \leq 1$. For two runs of CMA-MAE that generate the same sequence of m candidate solutions $\{S\} = \theta_1, \theta_2, \dots, \theta_m$, it follows that $f_{A_i}(\theta) \leq f_{A_j}(\theta)$ for all $\theta \in \mathbb{R}^n$.*

PROOF. We prove the theorem via induction over the sequence of solution additions. f_A is the histogram formed by the thresholds t_e over all archive cells e in the archive. Thus, we prove $f_{A_i} \leq f_{A_j}$ by showing that $t_e(A_i) \leq t_e(A_j)$ for all archive cells e after m archive additions.

As a basis step, we note that A_i equals A_j as both archives are initialized with \min_f .

Our inductive hypothesis states that after k archive additions we have $t_e(A_i) \leq t_e(A_j)$, and we need to show that $t_e(A_i) \leq t_e(A_j)$ after solution θ_{k+1} is added to each archive.

Our solution θ_{k+1} has three cases with respect to the acceptance thresholds:

Case 1: $f(\theta_{k+1}) \leq t_e(A_i) \leq t_e(A_j)$. The solution is not added to either archive and our property holds from the inductive hypothesis.

Case 2: $t_e(A_i) \leq f(\theta_{k+1}) \leq t_e(A_j)$. The solution is added to A_i , but not A_j , thus $t'_e(A_j) = t_e(A_j)$. We follow the threshold update: $t'_e(A_i) = (1 - \alpha_i)t_e(A_i) + \alpha_i f(\theta_{k+1})$. Next, we need to show that $t'_e(A_i) \leq t'_e(A_j)$ to complete the inductive step:

$$\begin{aligned} (1 - \alpha_i)t_e(A_i) + \alpha_i f(\theta_{k+1}) &\leq f(\theta_{k+1}) && \Longleftrightarrow \\ (1 - \alpha_i)t_e(A_i) &\leq (1 - \alpha_i)f(\theta_{k+1}) && \Longleftrightarrow \\ t_e(A_i) &\leq f(\theta_{k+1}) \text{ as } 1 - \alpha_i \geq 0 \end{aligned}$$

The last inequality holds true per our initial assumption for Case 2. From the inductive hypothesis, we have $f(\theta_{k+1}) \leq t_e(A_j) = t'_e(A_j)$.

Case 3: $t_e(A_i) \leq t_e(A_j) \leq f(\theta_{k+1})$. The solution θ_{k+1} is added to both archives. We need to show that $t'_e(A_i) \leq t'_e(A_j)$:

$$\begin{aligned} t'_e(A_i) &\leq t'_e(A_j) && \Longleftrightarrow \\ (1 - \alpha_i)t_e(A_i) + \alpha_i f(\theta_{k+1}) &\leq (1 - \alpha_j)t_e(A_j) + \alpha_j f(\theta_{k+1}) \end{aligned} \quad (9)$$

We can rewrite Eq. 9 as:

$$(1 - \alpha_j)t_e(A_j) - (1 - \alpha_i)t_e(A_i) + \alpha_j f(\theta_{k+1}) - \alpha_i f(\theta_{k+1}) \geq 0 \quad (10)$$

First, note that:

$$\begin{aligned} (1 - \alpha_j)t_e(A_j) - (1 - \alpha_i)t_e(A_i) &\geq (1 - \alpha_j)t_e(A_i) - (1 - \alpha_i)t_e(A_i) \\ &= (1 - \alpha_j - 1 + \alpha_i)t_e(A_i) \\ &= (\alpha_i - \alpha_j)t_e(A_i). \end{aligned}$$

Thus:

$$(1 - \alpha_j)t_e(A_j) - (1 - \alpha_i)t_e(A_i) \geq (\alpha_i - \alpha_j)t_e(A_i) \quad (11)$$

From Eq. 10 and 11 we have:

$$\begin{aligned} (1 - \alpha_j)t_e(A_j) + \alpha_j f(\theta_{k+1}) - (1 - \alpha_i)t_e(A_i) - \alpha_i f(\theta_{k+1}) \\ \geq (\alpha_i - \alpha_j)t_e(A_i) + (\alpha_j - \alpha_i)f(\theta_{k+1}) \\ = (\alpha_j - \alpha_i)(f(\theta_{k+1}) - t_e(A_i)) \end{aligned}$$

As $\alpha_j > \alpha_i$ and $f(\theta_{k+1}) \geq t_e(A_i)$, we have $(\alpha_j - \alpha_i)(f(\theta_{k+1}) - t_e(A_i)) \geq 0$. This completes the proof that Eq. 10 holds.

As all cases in our inductive step hold, our proof by induction is complete. \square

Finally, we wish to address the limitation that CMA-ME performs poorly on flat objectives, where all solutions have the same objective value. Consider how CMA-ME behaves on a flat objective $f(\theta) = C$ for all $\theta \in \mathbb{R}^n$, where C is an arbitrary constant. CMA-ME will only discover each new cell once and will not receive any further feedback from that cell, since any future solution cannot replace the incumbent elite. This hinders the CMA-ME's movement in measure space, which is based on feedback from *changes* in the archive. Future candidate solutions will only fall into occupied cells, triggering repeated restarts caused by CMA-ES's restart rule.

When the objective function plateaus, we still want CMA-ME to perform well and benefit from the CMA-ES adaptation mechanisms. One reasonable approach would be to keep track of the frequency o_e that each cell e has been visited in the archive, where o_e represents the number of times a solution was generated in that cell. Then, when a flat objective occurs, we rank solutions by descending frequency counts. Conceptually, CMA-ME would descend the density histogram defined by the archive, pushing the search towards regions of the measure space that have been sampled less frequently. Theorem. 5.4 shows that we obtain the density descent behavior on flat objectives *without additional changes to the CMA-MAE algorithm*.

To formalize our theory, we define the approximate density descent algorithm that is identical to CMA-ME, but differs by how solutions are ranked. Specifically, the algorithm maintains a histogram of occupancy counts o_e for each cell e , with o_e representing the number of times a solution was generated in that cell. This algorithm descends the density histogram in measure space by ranking solutions based on the

occupancy count of the cell that the solution maps to, where solutions that discover less frequently visited cells are ranked higher than more frequently visited cells. We will prove CMA-MAE and the approximate density descent algorithm are equivalent for flat objectives.

LEMMA E.5. *The threshold t_e after k additions to cell e forms a strictly increasing sequence for a constant objective function $f(\theta) = C$ for all $\theta \in \mathbb{R}^n$, when $0 < \alpha < 1$ and $\min_f < C$.*

PROOF. To show that t_e after k additions to cell e forms a strictly increasing sequence, we write a recurrence relation for t_e after k solutions have been added to cell e . Let $t_e(k) = (1 - \alpha)t_e(k - 1) + \alpha f(\theta_i)$ and $t_e(0) = \min_f$ be that recurrence relation. To show the recurrence is an increasing function, we need to show that $t_e(k) > t_e(k - 1)$ for all $k \geq 0$.

We prove the inequality via induction over cell additions k . As a basis step, we show $t_e(1) > t_e(0)$: $(1 - \alpha)\min_f + \alpha C > \min_f \iff \min_f - \min_f - \alpha \cdot \min_f + \alpha C \iff \alpha C > \alpha \cdot \min_f$. As $C > \min_f$ and $\alpha > 0$, the basis step holds.

For the inductive step, we assume that $t_e(k) > t_e(k - 1)$ and need to show that $t_e(k + 1) > t_e(k)$: $t_e(k + 1) > t_e(k) \iff (1 - \alpha)t_e(k) + \alpha C > (1 - \alpha)t_e(k - 1) + \alpha C \iff (1 - \alpha)t_e(k) > (1 - \alpha)t_e(k - 1) \iff t_e(k) > t_e(k - 1)$. \square

THEOREM E.6. *The CMA-MAE algorithm optimizing a constant objective function $f(\theta) = C$ for all $\theta \in \mathbb{R}^n$ is equivalent to the approximate density descent algorithm, when $0 < \alpha < 1$ and $\min_f < C$.*

PROOF. We will prove that for an arbitrary archive A with both the occupancy count for each cell o_e and the threshold value t_e computed with arbitrary learning rate $0 < \alpha < 1$, CMA-MAE results in the same ranking for an arbitrary batch of solutions $\{\theta_i\}$ as the approximate density descent algorithm.

We let θ_i and θ_j be two arbitrary solutions in the batch mapped to cells e_i and e_j . Without loss of generality, we let $o_{e_i} \leq o_{e_j}$. The approximate density descent algorithm will thus rank θ_i before θ_j . We will show that CMA-MAE results in the same ranking.

If $o_{e_i} \leq o_{e_j}$, and since t_e is a strictly increasing function from Lemma E.5: $t_{e_i}(o_{e_i}) \leq t_{e_j}(o_{e_j})$. We have $t_{e_i}(o_{e_i}) \leq t_{e_j}(o_{e_j}) \iff C - t_{e_i}(o_{e_i}) \geq C - t_{e_j}(o_{e_j})$. Thus, the archive improvement by adding θ_i to the archive is larger than the improvement by adding θ_j and CMA-MAE will rank θ_i higher than θ_j , identically with density descent. \square

While Theorem E.6 assumes a constant objective f , we conjecture that the theorem holds true generally when threshold t_e in each cell e approaches the local optimum within the cell boundaries.

CONJECTURE E.7. *The CMA-MAE algorithm becomes equivalent to the density descent algorithm for a subset of archive cells for an arbitrary convex objective f , where the cardinality of the subset of cells increases as the number of iterations increases.*

We provide intuition for our conjecture through the lense of the elite hypervolume hypothesis [79]. The elite hypervolume hypothesis states that optimal solutions for the MAP-Elites archive form a connected region in search space. Later work [68] connected the elite hypervolume hypothesis to the manifold hypothesis [19] in machine learning, stating that the elite hypervolume can be represented by a low dimensional manifold in search space.

For our conjecture, we assume that the elite hypervolume hypothesis holds and there exists a smooth manifold that represents the hypervolume. Next, we assume in the conjecture that f is an arbitrary convex function. As f is convex, early in the CMA-MAE search the discount function f_A will be flat and the search point θ will approach the global optimum following CMA-ES's convergence properties [38, 39], where the precision of convergence is controlled by archive learning rate α . By definition, the global optimum θ^* is within the elite hypervolume as no other solution of higher quality exists within its archive cell. Assuming the elite hypervolume hypothesis holds, a subset of adjacent solutions in search space will also be in the hypervolume due to the connectedness of the hypervolume. As f_A increases around the global optimum, we conjecture that the function $f(\theta^*) - f_A(\theta^*)$ will form a plateau around the optimum, since it will approach the value $f(\theta_i) - f_A(\theta_i)$ of adjacent solutions θ_i . By Theorem E.6 we have a density descent algorithm within the plateau, pushing CMA-MAE to discover solutions on the frontier of the known hypervolume.

Finally, we remark that our conjecture implies that $f - f_A$ tends towards a constant function in the limit, resulting in a density descent algorithm across the elite hypervolume manifold as the number of generated solutions approaches infinity. We leave a formal proof of this conjecture for future work.

F THEORETICAL PROPERTIES OF CMA-MAEGA

In this section, we investigate how the theoretical properties of CMA-MAE apply to CMA-MAEGA. While many of the properties are nearly a direct mapping, we note that, while CMA-MAE is equivalent to the single-objective optimization algorithm CMA-ES for $\alpha = 0$, there is no single-objective counterpart to CMA-MAEGA. To make the direct mapping easier, we introduce a counterpart: the gradient arborescence ascent algorithm.

The gradient arborescence ascent algorithm is similar to CMA-MEGA, but without an archive. Like CMA-MEGA, the algorithm assumes a differentiable objective f and differentiable measures \mathbf{m} . However, the algorithm leverages the objective and measure function gradients only to improve the optimization of the objective f , rather than to find solutions that are diverse with respect to measures \mathbf{m} . As with CMA-MEGA, the gradient arborescence algorithm branches in objective-measure space. However, the algorithm ranks solutions purely by the objective function f and adapts the coefficient distribution $N(\mu, \Sigma)$ towards the natural gradient of the objective f .

Next, we prove properties of CMA-MAEGA that directly follow from the properties of CMA-MAE.

THEOREM F.1. *The gradient arborescence ascent algorithm is equivalent to CMA-MAEGA when $\alpha = 0$, if gradient arborescence ascent restarts from an archive elite.*

PROOF. We note that CMA-MAEGA and the gradient arborescence ascent algorithm differ only in how they rank solutions, and we note that the differences between CMA-MAE and CMA-ES mirror the differences between CMA-MAEGA and gradient arborescence ascent algorithm. So by directly adapting the proof of Theorem E.1, we complete our proof. \square

THEOREM F.2. *The CMA-MEGA algorithm is equivalent to CMA-MAEGA when $\alpha = 1$ and \min_f is an arbitrarily large negative number.*

PROOF. We note that CMA-MAEGA and the CMA-MEGA algorithm differ only in how they rank solutions and how they update the archive A , and we note that the differences between CMA-MAE and CMA-ME mirror the differences between CMA-MAEGA and CMA-MEGA. So by directly adapting the proof of Theorem E.3, we complete our proof. \square

THEOREM F.3. *Let α_i and α_j be two archive learning rates for archives A_i and A_j such that $0 \leq \alpha_i < \alpha_j \leq 1$. For two runs of CMA-MAEGA that generate the same sequence of m candidate solutions $\{S\} = \theta_1, \theta_2, \dots, \theta_m$, it follows that $f_{A_i}(\theta) \leq f_{A_j}(\theta)$ for all $\theta \in \mathbb{R}^n$.*

PROOF. We note that CMA-MAE and CMA-MAEGA update the archive A in exactly the same way. Therefore, the proof follows directly by adapting the proof of Theorem E.4 to CMA-MAEGA. \square

Next, we wish to show that CMA-MAEGA results in density descent in measure space. However, we need a counterpart to the approximate density descent algorithm we defined in Theorem E.6.

Consider an approximate density descending arborescence algorithm that is identical to CMA-MEGA, but differs by how solutions are ranked. Specifically, we assume that this algorithm maintains an occupancy count o_e for each cell e , which is the number of times a solution was generated in that cell. The density descent algorithm ranks solutions based on the occupancy count of the cell that the solution maps to, where solutions that discover less frequently visited cells are ranked higher. The algorithm takes steps in search space \mathbb{R}^n that minimize the approximate density function defined by the archive and adapts the coefficient distribution $N(\mu, \Sigma)$ towards coefficients that minimize the density function.

THEOREM F.4. *The CMA-MAEGA algorithm optimizing a constant objective function $f(\theta) = C$ for all $\theta \in \mathbb{R}^n$ is equivalent to the approximate density descending arborescence algorithm, when $0 < \alpha < 1$ and $\min_f < C$.*

PROOF. The proof of Theorem E.6 relies only on how CMA-MAE updates the archive A and acceptance threshold t_e . The proof of this theorem follows directly by adapting the proof of Theorem E.6 to CMA-MAEGA. \square

G DERIVATION OF THE CONVERSION FORMULA FOR THE ARCHIVE LEARNING RATE

In this section, we derive the archive learning rate conversion formula $\alpha_2 = 1 - (1 - \alpha_1)^r$ mentioned in Section 7 of the main paper, where r is the ratio between archive cell counts, and α_1 and α_2 are archive learning rates for two archives A_1 and A_2 .

Given an archive learning rate α_1 for A_1 , we want to derive an equivalent archive learning rate α_2 for A_2 that results in robust performance when CMA-MAE is run with either A_1 or A_2 . A principled way to derive a conversion formula for α_2 is to look for an invariance property that affects the performance of CMA-MAE and that holds when CMA-MAE generates solutions in archives A_1 and A_2 .

Since CMA-MAE ranks solutions by $f - f_A$, we wish for f_A to increase at the same rate in the two archives. Since $f_A(\theta) = t_e$, where t_e is the cell that a solution θ maps to, we select the *average value* of the acceptance thresholds t_e over all cells in each archive as our invariant property.

We assume an arbitrary sequence of N solution additions $\theta_1, \theta_2, \dots, \theta_N$, evenly dispersed across the archive cells. We then specify t_e as a function that maps k cell additions to a value t_e in archive cell e .⁴ Equation 12 then defines the average value of t_e across the archive after N additions to an archive A with M cells.

$$\frac{1}{M} \sum_{i=1}^M t_e \left(\frac{N}{M} \right) \quad (12)$$

Then, equation 13 defines the invariance we want to guarantee between archives A_1 and A_2 .

$$\frac{1}{M_1} \sum_{i=1}^{M_1} t_e \left(\frac{N}{M_1} \right) = \frac{1}{M_2} \sum_{i=1}^{M_2} t_e \left(\frac{N}{M_2} \right) \quad (13)$$

In Eq. 13, we let M_1 and M_2 the number of cells in archives A_1 and A_2 , and we assume that M_1 and M_2 divide N . To solve for a closed form of α_2 subject to our invariance, we need a formula for the function t_e . Similar to Lemma E.5, we can represent the function t_e as a recurrence relation after adding k solutions to cell e of an archive A .

⁴Here we abuse notation and view t_e as a function instead of threshold for simplicity and to highlight the connection to the threshold value t_e .

$$\begin{aligned} t_e(0) &= \min_f \\ t_e(k) &= (1 - \alpha)t_e(k-1) + \alpha f(\theta_k) \end{aligned} \quad (14)$$

Next, we look to derive a closed form for $t_e(k)$ for an archive A as a way to manipulate Equation 13. However, solving for $t_e(k)$ when f is an arbitrary function is difficult, because different regions of the archive will change at different rates. Instead, we solve for the special case when $f(\theta) = C$ and $\min_f < C$, where $C \in \mathbb{R}$ is a constant scalar. To solve for a closed form of the recurrence $t_e(k)$, we leverage the recurrence unrolling method [30], allowing us to guess the closed form in Equation 15.

$$\begin{aligned} t_e(1) &= (1 - \alpha)t_e(0) + \alpha C = (1 - \alpha)\min_f + \alpha C \\ t_e(2) &= (1 - \alpha)t_e(1) + \alpha C = (1 - \alpha)[(1 - \alpha)\min_f + \alpha C] + \alpha C \\ &= (1 - \alpha)^2\min_f + (1 - \alpha)\alpha C + \alpha C \\ t_e(3) &= (1 - \alpha)t_e(2) + \alpha C \\ &= (1 - \alpha)[(1 - \alpha)^2\min_f + (1 - \alpha)\alpha C + \alpha C] + \alpha C \\ &= (1 - \alpha)^3\min_f + (1 - \alpha)^2\alpha C + (1 - \alpha)\alpha C + \alpha C \\ &\vdots \\ t_e(k) &= (1 - \alpha)^k\min_f + \sum_{i=0}^{k-1} (1 - \alpha)^i \alpha C \end{aligned} \quad (15)$$

We recognize the summation in Equation 15 as a geometric series. As $0 < \alpha < 1$, we rewrite the summation as follows.

$$\begin{aligned} t_e(k) &= (1 - \alpha)^k\min_f + \sum_{i=0}^{k-1} (1 - \alpha)^i \alpha C \\ &= (1 - \alpha)^k\min_f + \alpha C \left(\frac{1 - (1 - \alpha)^k}{1 - (1 - \alpha)} \right) \\ &= (1 - \alpha)^k\min_f + \alpha C \left(\frac{1 - (1 - \alpha)^k}{\alpha} \right) \\ &= (1 - \alpha)^k\min_f + C - C(1 - \alpha)^k \\ &= (\min_f - C)(1 - \alpha)^k + C \\ &= C - (C - \min_f)(1 - \alpha)^k \end{aligned} \quad (16)$$

Next, we prove that the closed form we guessed is the closed form of the recurrence relation.

THEOREM G.1. *The recurrence relation $t_e(0) = \min_f$ and $t_e(k) = (1 - \alpha)t_e(k-1) + \alpha C$ has the closed form $t_e(k) = C - (C - \min_f)(1 - \alpha)^k$, where $0 < \alpha < 1$ and $\min_f < C$.*

PROOF. We show the closed form holds via induction over cell additions k .

As a basis step we show that $t_e(0) = C - (C - \min_f)(1 - \alpha)^0 = C - (C - \min_f) = \min_f$.

For the inductive step, suppose after j insertions into the archive A in cell e our closed form holds. We show that the closed form holds for $j + 1$ insertions.

$$\begin{aligned} t_e(j+1) &= (1 - \alpha)t_e(j) + \alpha C \\ &= (1 - \alpha)[C - (C - \min_f)(1 - \alpha)^j] + \alpha C \\ &= C(1 - \alpha) - (C - \min_f)(1 - \alpha)^{j+1} + \alpha C \\ &= C - \alpha C + \alpha C - (C - \min_f)(1 - \alpha)^{j+1} \\ &= C - (C - \min_f)(1 - \alpha)^{j+1} \end{aligned} \quad (17)$$

As our basis and inductive steps hold, our proof is complete. \square

The closed form from Theorem G.1 allows us to derive a conversion formula for α_2 via our invariance formula in Equation 13.

$$\begin{aligned}
\frac{1}{M_1} \sum_{i=1}^{M_1} t_e \left(\frac{N}{M_1} \right) &= \frac{1}{M_2} \sum_{i=1}^{M_2} t_e \left(\frac{N}{M_2} \right) \\
\frac{M_1}{M_1} \left(C - (C - \min_f)(1 - \alpha_1)^{\frac{N}{M_1}} \right) &= \frac{M_2}{M_2} \left(C - (C - \min_f)(1 - \alpha_2)^{\frac{N}{M_2}} \right) \\
(C - \min_f)(1 - \alpha_1)^{\frac{N}{M_1}} &= (C - \min_f)(1 - \alpha_2)^{\frac{N}{M_2}} \\
(1 - \alpha_1)^{\frac{N}{M_1}} &= (1 - \alpha_2)^{\frac{N}{M_2}} \\
(1 - \alpha_1)^{\frac{M_2}{M_1}} &= (1 - \alpha_2) \\
\alpha_2 &= 1 - (1 - \alpha_1)^{\frac{M_2}{M_1}} \tag{18}
\end{aligned}$$

We remark that our conversion formula is not dependent on the number of archive additions N . Although our conversion formula assumes f to be a constant objective, we conjecture that the formula holds generally for a convex objective f .

CONJECTURE G.2. *The archive learning rate conversion formula results in invariant behavior of CMA-MAE for two arbitrary archives A_1 and A_2 with archive resolutions M_1 and M_2 , for a convex objective f .*

Our intuition is similar to the intuition behind Conjecture E.7, where we assume the elite hypervolume hypothesis holds [79]. At the beginning of the CMA-MAE search, f_A is a constant function and CMA-MAE optimizes for the global optimum, following the convergence properties of CMA-ES [38, 39]. Eventually, the cells around the global optimum become saturated and the function $f - f_A$ forms a plateau around the global optimum. The invariance described in Eq. 13 implies that the f_{A_1} and f_{A_2} will increase at the same rate within the flat region of the plateau. Let θ_p be an arbitrary solution in the plateau and θ' be a solution on the frontier of the known hypervolume. The plateau of each archive A_i expands when the solutions on the frontier of the elite hypervolume achieve a larger $f(\theta') - f_{A_i}(\theta')$ than the plateau $f(\theta_p) - f_{A_i}(\theta_p)$. We conjecture that the plateau will expand at the same rate in the two archives as f_{A_1} and f_{A_2} increase at the same rate for the plateau region, due to our invariance in Eq. 13.

We speculate that our conjecture explains why we observe invariant behavior across archive resolutions in the experiments of Section 7, even though f is not a constant function in the linear projection and arm repertoire domains.

H A BATCH THRESHOLD UPDATE RULE FOR MAP-ANNEALING

In this paper, we presented an annealing method for updating a QD archive in the CMA-MAE algorithm, following the standard QD formulation where we add a single solution to the archive at a time. However, the recently developed QDax library [56] assumes that the updates to the archive happen in batch. In this section, we show that the archive update within a batch is dependent on the order that the solutions are processed. We then propose a candidate threshold update rule that is invariant to the order the solutions are processed within a batch update.

First, we show that the order solutions are added to the archive affects the current threshold update. Consider two solutions θ_1 and θ_2 that we add to the archive in a single batch. If θ_1 is added before θ_2 , then the threshold update becomes $t'_e = (1 - \alpha)[(1 - \alpha)t_e + \alpha f(\theta_1)] + \alpha f(\theta_2) = (1 - \alpha)^2 t_e + (1 - \alpha)\alpha f(\theta_1) + \alpha f(\theta_2)$. If θ_2 is added before θ_1 , then the threshold update becomes $t''_e = (1 - \alpha)[(1 - \alpha)t_e + \alpha f(\theta_2)] + \alpha f(\theta_1) = (1 - \alpha)^2 t_e + (1 - \alpha)\alpha f(\theta_2) + \alpha f(\theta_1)$.

To compare t'_e to t''_e , we compute $t'_e - t''_e$:

$$\begin{aligned}
t'_e - t''_e &= (1 - \alpha)^2 t_e + (1 - \alpha)\alpha f(\theta_1) + \alpha f(\theta_2) \\
&= [(1 - \alpha)^2 t_e + (1 - \alpha)\alpha f(\theta_2) + \alpha f(\theta_1)] \\
&= (1 - \alpha)\alpha [f(\theta_1) - f(\theta_2)] + \alpha [f(\theta_2) - f(\theta_1)] \\
&= [(1 - \alpha)\alpha - \alpha] [f(\theta_1) - f(\theta_2)] \\
&= -\alpha^2 [f(\theta_1) - f(\theta_2)]
\end{aligned}$$

From the above derivation, we see that the difference between thresholds is dependent on the solution's objective values when added to the archive in different order. This means when adding solutions to the archive in a batch, the update is dependent on the solution order in the batch.

Our goal is to make the threshold update invariant to the order the solutions are added to the archive. First, consider a subset of the batch that contains c solutions all landing in the same cell of the archive and exceeding the current threshold t_e . Adding the solutions in batch order results in the following threshold update:

$$t'_e = (1 - \alpha)^c t_e + \sum_{j=1}^c (1 - \alpha)^{c-j} \alpha f(\theta_j)$$

Let X be a random variable corresponding to the threshold for a given permutation of the batch. To become invariant to the batch addition, we will change the threshold update to be $\mathbb{E}[X]$, the expected value of t'_e across all random permutations of the batch.

Let X_i be a random variable corresponding to the contribution of only $f(\theta_i)$ to the threshold update and Y be a constant random variable corresponding to the contribution of the previous threshold. As expectation is linear, we have $\mathbb{E}[X] = \mathbb{E}[Y] + \sum_{j=1}^c \mathbb{E}[X_j]$. Next, we compute the value of $\mathbb{E}[X_i]$ for an arbitrary solution θ_i in the batch:

$$\begin{aligned} \mathbb{E}[X_i] &= \sum_{j=1}^c \Pr(\theta_i \text{ is at position } j \text{ in the batch}) (1 - \alpha)^{c-j} \alpha f(\theta_i) \\ &= \sum_{j=1}^c \frac{(c-1)!}{c!} (1 - \alpha)^{c-j} \alpha f(\theta_i) \\ &= \sum_{j=1}^c \frac{1}{c} (1 - \alpha)^{c-j} \alpha f(\theta_i) \end{aligned}$$

Next, we rework $\mathbb{E}[X]$ into a simpler formula, where $f^* = \frac{\sum_{k=1}^c f(\theta_k)}{c}$:

$$\begin{aligned} \mathbb{E}[X] &= \mathbb{E}[Y] + \sum_{j=1}^c \mathbb{E}[X_j] \\ &= (1 - \alpha)^c t_e + \sum_{k=1}^c \sum_{j=1}^c \frac{1}{c} (1 - \alpha)^{c-j} \alpha f(\theta_k) \\ &= (1 - \alpha)^c t_e + \sum_{j=1}^c (1 - \alpha)^{c-j} \alpha \frac{1}{c} \sum_{k=1}^c f(\theta_k) \\ &= (1 - \alpha)^c t_e + \sum_{j=1}^c (1 - \alpha)^{c-j} \alpha f^* \\ &= (1 - \alpha)^c t_e + \alpha f^* \sum_{j=0}^{c-1} (1 - \alpha)^j \\ &= (1 - \alpha)^c t_e + \alpha f^* \frac{1 - (1 - \alpha)^c}{\alpha} \\ &= (1 - \alpha)^c t_e + f^* (1 - (1 - \alpha)^c) \end{aligned}$$

We propose the above expectation as the batch threshold update rule, where f^* is the average objective value for all solutions in the batch that exceed the threshold t_e for a given cell. We observe that the rule is independent of the solution order. Furthermore, if $\alpha = 0$, the update becomes t_e , and Theorem 5.1 still holds. If $\alpha = 1$, the update becomes f^* , which is the average of solutions that increase the threshold. We view this update as a smooth parallel addition compared to CMA-ME, which would add the best solution from the batch for any solution order. On flat objectives, we note that all permutations of a batch result in the same threshold after processing the batch, and a sequential threshold update is equivalent to the expected threshold update of our batch update. Therefore, Theorem 5.4 holds for our batch threshold update rule due to the batch update being the same as the sequential update in this case. We leave exploring alternative batch update rules for future work.

I ON IMPROVING THE QUALITY OF LATENT SPACE ILLUMINATION

We describe the limitations arising from the exact problem setup for LSI (StyleGAN) domain, adopted from previous work [21], on producing high-quality images. We then discuss ideas from the generative art community for improving the setup and an additional experiment that incorporates these ideas to generate high-quality and diverse images.

I.1 Main LSI Experiments

In the main latent space illumination (LSI) experiments in section 6, we showed that CMA-MAE outperformed the other QD algorithms according to standard QD metrics following the exact setup of prior work [21].

In these experiments, we used latent space illumination as purely an optimization benchmark. However, obtaining high performance on LSI as a benchmark can be a competing objective with producing high quality images.

First, finding solutions that result in a high objective value does not always result in high quality images that match the text prompt. For example, a QD algorithm can find images that result in CLIP reporting a high similarity score by leaving the training distribution of StyleGAN.

Furthermore, we use the CLIP loss as a measure function, thus a QD algorithm attempts to both decrease and increase the loss function to cover the measure space. Increasing the loss function results in minimizing similarity with the text prompt, which can be attained by unrealistic images.

In the main LSI experiments all derivative-free QD algorithms would drift out of the latent distribution and produce archives of low image quality. We found that CMA-MAE would stay in the latent distribution longer before drifting out of distribution during exploration, due to the low archive learning rate α prioritizing the objective.

To address drifting out of distribution, we adopt a “timeout” restart rule proposed by other evolution strategy-based quality diversity algorithms [10, 62]. A timeout restart rule runs for a fixed number of iterations before restarting. We add to the basic restart rule of CMA-MAE (Appendix A) an additional criterion for restarting based on the timeout restart rule. To generate all the LSI collages in section L, we use a timeout of 50 iterations for both CMA-MAE and CMA-MAEGA.

While we retained the same setup as in previous work for comparison purposes, we can change the setup by adopting ideas from the generative art community to produce very high quality images. We describe these ideas in section I.2.

I.2 Innovations from the Generative AI Art Community

Beyond the specifics of the QD optimization algorithm, many aspects of latent space illumination can be improved. For example, prior work [27] on guiding single-objective optimization with CLIP notes that the gradients that CLIP provides can be noisy and recommends data augmentations of the generated images, such as tiling or translating each image, before being passed to CLIP. This change can help smooth the gradients for gradient descent optimizers like Adam and can make the generated images retained by the archive match their text prompts more accurately.

Prior work on optimizing the latent space of VQ-GAN [12] also notes that CLIP will not always provide smooth optimization gradients, nor accurate objective values. The authors recommend a different data augmentation, by creating a batch of random cutouts of the generated image and passing those images to CLIP, which produces smoother gradients and objective values. The paper also recommends regularizing the latent codes so that they become attracted to the Gaussian ball that captures the training distribution of the GAN. Both these techniques could improve the qualitative performance of latent space illumination.

Finally, we used the first version of StyleGAN [46] that was used in prior work [21]. Recent versions of StyleGAN [44, 45, 47] can further improve the quality of the generated images.

We describe details of the improved setup in section I.3.

I.3 Improving Quality of Generated Images

To improve image quality, we include an additional experiment where we run each QD algorithm with a configuration inspired by the above findings from the generative art community.

First, we replace StyleGAN [46] with StyleGAN2 [47], which produces better images and has a well-conditioned latent space for optimization. Next, we change the latent space being optimized by QD. First note, that the StyleGAN architecture has multiple latent spaces to be optimized. StyleGAN consists of both a z -space latent space of size 512 and a mapping network that maps to 18 latent codes of size 512 at different levels of detail in the final image. This 18×512 tensor is known as w -space. The original LSI experiments [21] were based of a blogpost [64] that represented the search space for LSI as a single 512 dimensional vector whose weights were shared for each level of detail in w -space. In this experiment, we will optimize the full $n = 18 \times 512 = 9216$ w -space with each QD algorithm for fine grain control of the generated images.

Instead of using restarts in the StyleGAN experiments to keep the search within latent space, we adopt the w -space regularization [12]. We compute an average w -space position by sampling 10^4 points sampled from $\mathcal{N}(0, I)$ in z -space, then passing these points through the mapping network to find their position in w -space. We compute the standard error across each dimension. To regularize the latent space, we compute the distance from this w -space Gaussian distribution. If the distance from mean exceeds the Gaussian ball of highest density, we apply an L2 penalty to the objective f to move the search back into the training distribution.

The LSI experiments from prior work [21] downsample from the 1024×1024 images produced by StyleGAN to the 224×224 images required for input to the CLIP model. Following prior work [12], we adopt the cutout technique that clips 32 images from the StyleGAN output of varying sizes, downsamples each cutout to 224×224 , and passes each of these 224×224 cutouts to CLIP for evaluation. The loss becomes the average of the CLIP loss for all cutouts. This technique has been shown to smooth gradients for CLIP in single-objective latent space optimization.

Instead of starting the search at the latent code $\mathbf{0}$, we sample 512 latent codes from $\mathcal{N}(0, I)$ in z -space then select the image resulting in the highest objective value as the starting w -space latent code.

Finally, the prior LSI experiments leveraged the text prompt “A small child.” as a proxy for age. However, this text prompt only specifies one end of the age measure. To correct this issue, we can pair a positive text prompt “A small child.” with a negative text prompt “An elderly person.” as a proxy for age. We compute the measure output by subtracting one CLIP loss from the other.

We run the improved LSI experiment with the text descriptor “A photo of the face of Tom Cruise.” as an objective, the text pair “A photo of Tom Cruise as a small child.” and “A photo of Tom Cruise as an elderly person.” as a proxy measure for age, and “A photo of Tom Cruise with short hair.” and “A photo of Tom Cruise with long hair.” as a proxy measure for hair length.

Fig. 4 shows photos of Tom Cruise at varying hair lengths and ages, generated by the CMA-MAEGA algorithm in a single run.

J ON THE EFFECT OF THRESHOLD INITIALIZATION

In this paper we introduce two hyperparameters for our proposed CMA-MAE algorithm: the archive learning rate α and a threshold initialization \min_f . In this section we discuss the effect of different \min_f initializations on the performance and behavior of CMA-MAE. Finally, we run an ablation on \min_f , similar to the ablation on archive learning rate α in Section 7.

First, consider the effect of \min_f on the extreme cases of the CMA-MAE. When $\alpha = 0$, then according to Theorem E.1, CMA-MAE behaves identically to CMA-ES, and \min_f has no effect on the behavior of CMA-MAE. Conversely when $\alpha = 1$, then according to Theorem E.3, CMA-MAE behaves identically to CMA-ME when \min_f approaches an arbitrarily large negative number. As \min_f increases for $\alpha = 1$, CMA-MAE will rank some solutions that discover existing cells higher than solutions that discover new, empty cells, thus it will behave differently than CMA-ME.

Next, we discuss the behavior for $0 < \alpha < 1$. Recall the elite hypervolume hypothesis [19], which states that optimal solutions for the MAP-Elites archive form a connected region in search space, the elite hypervolume. According to the proof sketch of Conjecture E.7, early in the search CMA-MAE behaves identically to CMA-ES to find a solution point on the elite hypervolume. As the thresholds of cells around this solution point become saturated, the objective $f - f_A$ forms a plateau around the local optimum. Within the plateau, CMA-MAE triggers the density descent property of Theorem E.6 and evenly explores the known elite hypervolume until the plateau in $f - f_A$ dips below the frontier of the known hypervolume. This causes the known hypervolume to expand until all cells of the archive are filled.

Next, we discuss how the selection of \min_f affects the rate of expansion of the elite hypervolume. First, we consider two solution points: θ_1 represents a local optimum in the elite hypervolume and θ_2 represents a nearby point mapped to a different archive cell with a smaller objective value, or formally $f(\theta_1) > f(\theta_2)$ and $\|\theta_1 - \theta_2\|_2 \leq \epsilon$. We let $f_A(\theta_1) = t_{e_1}$ and $f_A(\theta_2) = t_{e_2}$, where t_{e_1} and t_{e_2} represent the thresholds of the cells that θ_1 and θ_2 map to, respectively. Both thresholds t_{e_1} and t_{e_2} are initialized with \min_f .

We first examine the case where $\min_f > f(\theta_1) > f(\theta_2)$. Here, the thresholds t_{e_1} and t_{e_2} will not change and none of the two solutions points will be added to the archive. CMA-MAE will then only optimize for the objective value and behave identically to CMA-ES.

The second case is $f(\theta_1) > \min_f > f(\theta_2)$. Here, θ_2 will not get added to the archive and $t_{e_2} = \min_f$ will not change, while t_{e_1} will increase based on the update rule $t_{e_1} \leftarrow (1 - \alpha)t_{e_1} + f(\theta_1)$. Recall that CMA-MAE ranks solutions based on improvement $\Delta_i = f(\theta_i) - t_{e_i}$. We observe that $\Delta_2 = f(\theta_2) - \min_f < 0$, while $\Delta_1 = f(\theta_1) - t_{e_1} > 0$, thus there is no incentive for CMA-MAE to optimize for θ_2 and it will instead optimize for the solution point θ_1 that has the highest objective value. We observe that \min_f then acts as a constraint that prevent exploration of measure space regions with objective values below \min_f .

Finally, we let $f(\theta_1) > f(\theta_2) > \min_f$. Initially, θ_1 will be ranked higher than θ_2 , since $\Delta_1 = f(\theta_1) - t_{e_1} = f(\theta_1) - \min_f$ and $\Delta_2 = f(\theta_2) - t_{e_2} = f(\theta_2) - \min_f$, thus $\Delta_1 > \Delta_2$. CMA-MAE will thus optimize for θ_1 , but Δ_1 will decrease because of the update rule $t_{e_1} \leftarrow (1 - \alpha)t_{e_1} + f(\theta_1)$.

Next, we compute how many steps it will take for $\Delta_1 = \Delta_2$. When $\Delta_1 = \Delta_2$, a plateau forms for $f - f_A$ and CMA-MAE transitions from optimizing like CMA-ES to expanding the frontier of the known hypervolume via density descent. We leverage Theorem G.1 that yields a closed form for updating a cell k times for a fixed objective value C : $t_e(k) = C - (C - \min_f)(1 - \alpha)^k$.

Let k_1 and k_2 be the number of times the cells containing θ_1 and θ_2 are sampled, respectively. We note that CMA-MAE behaves like CMA-ES until we reach the density descent property, therefore the cell containing θ_1 will be sampled more times than the cell containing θ_2 and $k_1 > k_2$, where the gap $k_1 - k_2$ grows as more optimization steps are taken.

	LP (sphere)		LP (Rastrigin)		LP (plateau)		Arm Repertoire	
\min_f (CMA-MAE)	QD-score	Coverage	QD-score	Coverage	QD-score	Coverage	QD-score	Coverage
-80	64.74	83.73%	52.23	81.65%	77.20	77.24%	78.97	79.25%
-40	64.94	83.83%	52.53	81.40%	78.25	78.28%	79.02	79.26%
0	64.99	83.52%	52.69	80.56%	79.29	79.31%	79.06	79.27%
40	63.82	80.08%	48.61	68.45%	80.18	80.19%	79.06	79.23%
80	39.41	43.92%	10.03	11.04%	81.42	81.42%	78.99	79.11%

Table 4: Mean QD metrics after 10,000 iterations for CMA-MAE with varying \min_f initialization.

$$\begin{aligned}
\Delta_1 &= \Delta_2 \\
f(\theta_1) - t_{e_1} &= f(\theta_2) - t_{e_2} \\
f(\theta_1) - [f(\theta_1) - (f(\theta_1) - \min_f)(1 - \alpha)^{k_1}] &= f(\theta_2) - [f(\theta_2) - (f(\theta_2) - \min_f)(1 - \alpha)^{k_2}] \\
(f(\theta_1) - \min_f)(1 - \alpha)^{k_1} &= (f(\theta_2) - \min_f)(1 - \alpha)^{k_2} \\
\frac{(1 - \alpha)^{k_1}}{(1 - \alpha)^{k_2}} &= \frac{f(\theta_2) - \min_f}{f(\theta_1) - \min_f} \\
(1 - \alpha)^{k_1 - k_2} &= \frac{f(\theta_2) - \min_f}{f(\theta_1) - \min_f} \\
k_1 - k_2 &= \frac{\log \frac{f(\theta_2) - \min_f}{f(\theta_1) - \min_f}}{\log (1 - \alpha)} \\
k_1 - k_2 &= \frac{\log \frac{f(\theta_1) - \min_f}{f(\theta_2) - \min_f}}{-\log (1 - \alpha)} \tag{19}
\end{aligned}$$

We note that $-\log (1 - \alpha)$ is a positive value as $1 - \alpha < 1$. We see that the number of times that θ_1 needs to be sampled more than θ_2 depends on the log ratio of the gaps between the objective values and \min_f and on the learning rate α .

As \min_f decreases, number of optimization steps required to reach the plateau property approaches 0 asymptotically. While this shows that \min_f does have an effect on the behavior of the algorithm, since \min_f appears on the log ratio, we expect the effect of changing \min_f to be small.

We ran an ablations study by varying \min_f on the linear projection and arm repertoire domains. We explore different values of $\min_f \in \{-80, -40, 0, 40, 80\}$. We ran each experimental setup for 20 trials each and report the results in Table 4.

We note that each domain remaps the objective values to the range $[0, 100]$. For \min_f smaller than the range, we observe that changing \min_f has a negligible effect on performance. On the other hand, positive values for \min_f constrain the search to solutions with $f \geq \min_f$ (see Fig. 9), thus coverage decreases. These results match our theoretical analysis.

We note that in the LP (plateau) all optimal solutions for each cell are 100 and Arm Repertoire domain all optimal solutions for each cell are close to 100. Since all \min_f values in our range are below 100, we do not observe any effects on performance, even for positive values of \min_f .

K ON THE EFFECTS OF HIGH SEARCH SPACE DIMENSIONALITY AND HEAVY DISTORTION

In this section, we investigate the performance of CMA-MAE on high-dimensional versions of the linear projection and arm repertoire domains and discuss the performance of CMA-MAE when the projection from search space to measure space is heavily distorted. In the main experiments of the paper, we ran the linear projection and arm repertoire domains following the configuration from the CMA-ME paper [26]. In the CMA-ME paper each domain was run on $n = 20$ and $n = 100$ search spaces, and we adopted the more challenging $n = 100$ search spaces. However, later work [21] replicated these domains with $n = 1000$ search spaces to show the benefits of DQD algorithms on high-dimensional problems. The authors noted the poor performance of CMA-ME on the 1000-dimension version of the linear projection domain. In Appendix G of the DQD paper [21], the authors explored running the linear projection experiments with a 500×500 archive resolution. For a higher resolution archive, CMA-ME outperformed MAP-Elites and MAP-Elites (line).

Invariance to Archive Resolution. This paper proposes CMA-MAE, the first QD algorithm invariant to archive resolution. As a result, we wish to understand how CMA-MAE performs at different archive resolutions on high-dimensional search spaces, such as the 1000-dimensional linear projection domain. As an initial experiment, we run each derivative-free QD algorithm on the linear projection and arm repertoire domain varying from 50×50 resolution to 500×500 resolution. We linearly vary the cells along each dimension with 10 different archive

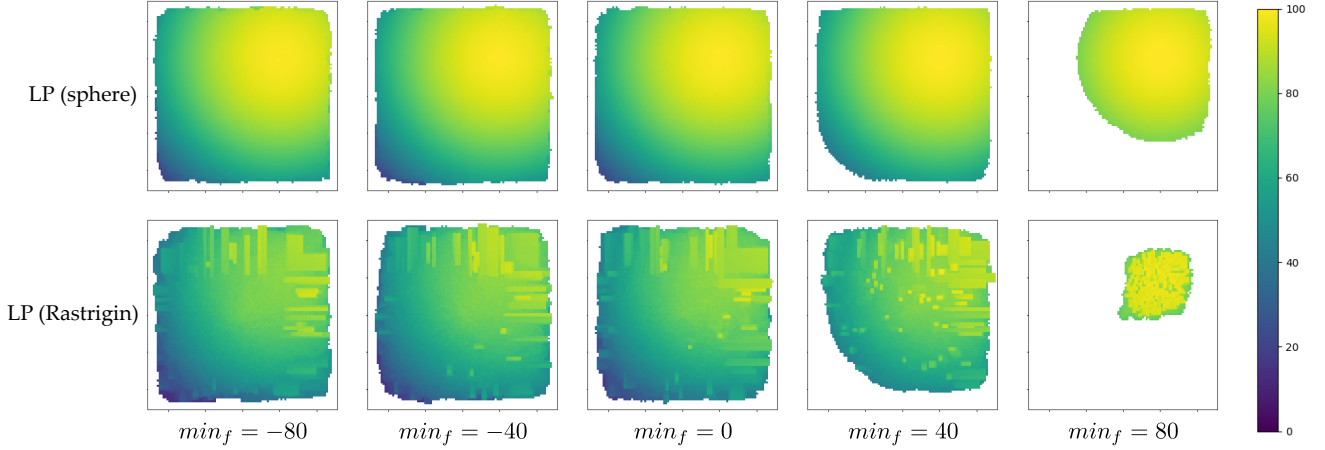


Figure 9: Example heatmaps from the \min_f ablation. When \min_f exceeds the objective value for solutions in the elite hypervolume, \min_f acts as a constraint on exploration and CMA-MAE focuses on regions of the elite hypervolume that exceed \min_f in objective value.

resolutions. Like the experiments for $n = 100$, we set the archive learning rate $\alpha = 0.01$ and apply the conversion formula from Appendix G to find equivalent α for different archive resolutions. We run one trial for each archive resolution and algorithm combination.

Figure 10 visualizes the results of the resolution experiment. On the linear projection domains, we observe a performance cliff for CMA-MAE for archive resolutions under 200×200 . For resolutions 200×200 and above, we observe the archive resolution invariant behavior of CMA-MAE. MAP-Elites (line) performs best on 100×100 archives with a performance drop for smaller or larger archives. CMA-ME and MAP-Elites both struggle on these domains at any archive resolution, but improve performance as archive resolution increases. For the arm repertoire domain, we observe invariant behavior for CMA-MAE. Both MAP-Elites variants decline in performance as archive resolution increases. We observe erratic performance in CMA-ME across different archive resolutions.

To explain the performance cliff for CMA-MAE with low resolution archives on the linear projection domain, we must first consider the search space distortion caused by the Bates distribution (see Figure 6) of that domain, where the measure functions are equally dependent on each parameter of the search vector $\theta \in \mathbb{R}^n$. The Bates distribution shows that as n grows, the search space becomes compressed to an increasingly narrow region of measure space, causing heavy distortion. For $n = 1000$, large perturbations to search parameters results in small perturbations to measure space values. For low resolution archives, this causes a sampled population of solutions from a search space Gaussian to be projected to the same cell of the archive, even for a Gaussian of large variance. This violates a fundamental assumption in CMA-MAE and CMA-ME: sampled solutions fall into different cells in the archive. By occupying the same cell, CMA-MAE receives no information about how the search mean θ is moving through measure space. Without this information, CMA-MAE will not fill the archive evenly, an assumption made when deriving the learning rate conversion formula in Appendix G. A 200×200 archive is high enough resolution to ensure that solutions sampled from the initial Gaussian fall into different archive cells, thus this is the resolution at the edge of CMA-MAE’s performance cliff.

For the arm repertoire domain, we do not observe a performance cliff for CMA-MAE. We attribute this behavior to the arm repertoire domain having weaker distortion than the linear projection domain. In the arm repertoire domain, the (x, y) position of the robot gripper is not equally dependent on all joint angles of the robotic arm. Joint angles closer to the base of the arm have a large affect on the gripper than joint angles near the gripper. This results in weaker distortion in the arm repertoire domain than the linear projection domain, where sampled solutions occupy different archive cells even for low resolution archives.

Performance. For the second experiment, we evaluate each algorithm on the linear projection and arm repertoire domains for 300×300 resolution archives. We selected this resolution so it is beyond the performance cliff of CMA-MAE in Fig. 10. Table 5 presents the results of this experiment. For each domain, CMA-MAE outperforms all other derivative-free QD algorithms in both coverage and QD-score.

The results of both experiments suggest that the CMA-MAE algorithm scales to high-dimensional search spaces better than CMA-ME. However, special care must be taken in domains with heavy distortion, such as the linear projection domain, where the archive resolution must be granular enough to overcome the distortion. The results highlight an important caveat to CMA-MAE’s archive invariance: sampled solutions from the multivariate Gaussian must fall into *different* archive cells to achieve archive resolution invariance.

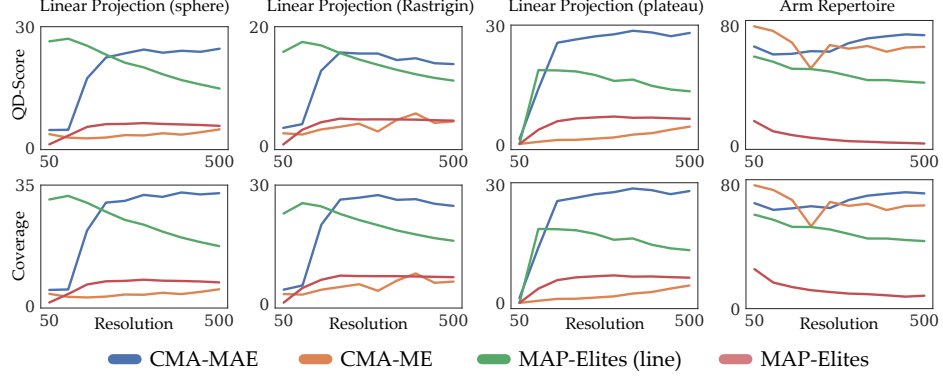


Figure 10: Final QD-score and coverage of each algorithm for 10 different archive resolutions on $n = 1000$ experiments.

Linear Projection (sphere)			
Algorithm	QD-score	Coverage	Best
MAP-Elites	6.11 ± 0.02	$7.53 \pm 0.03\%$	90.00 ± 0.02
MAP-Elites (line)	19.57 ± 0.04	$23.13 \pm 0.04\%$	96.61 ± 0.02
CMA-ME	3.26 ± 0.06	$3.40 \pm 0.06\%$	100.0 ± 0.00
CMA-MAE	24.43 ± 0.09	$32.34 \pm 0.11\%$	95.11 ± 0.17
Linear Projection (Rastrigin)			
Algorithm	QD-score	Coverage	Best
MAP-Elites	4.55 ± 0.01	$7.18 \pm 0.02\%$	74.62 ± 0.05
MAP-Elites (line)	13.69 ± 0.03	$19.98 \pm 0.05\%$	79.27 ± 0.03
CMA-ME	3.81 ± 0.12	$5.17 \pm 0.17\%$	90.79 ± 0.10
CMA-MAE	15.54 ± 0.15	$27.46 \pm 0.26\%$	89.93 ± 0.25
Linear Projection (plateau)			
Algorithm	QD-score	Coverage	Best
MAP-Elites	6.96 ± 0.03	$6.96 \pm 0.03\%$	100.00 ± 0.00
MAP-Elites (line)	16.51 ± 0.09	$16.51 \pm 0.09\%$	100.00 ± 0.00
CMA-ME	1.94 ± 0.07	$1.94 \pm 0.07\%$	100.00 ± 0.00
CMA-MAE	28.29 ± 0.14	$28.53 \pm 0.15\%$	100.00 ± 0.00
Arm Repertoire			
Algorithm	QD-score	Coverage	Best
MAP-Elites	3.12 ± 0.04	$9.76 \pm 0.09\%$	39.77 ± 0.16
MAP-Elites (line)	47.03 ± 0.18	$48.62 \pm 0.18\%$	97.34 ± 0.01
CMA-ME	65.66 ± 0.56	$67.27 \pm 0.57\%$	99.13 ± 0.00
CMA-MAE	68.85 ± 0.28	$70.52 \pm 0.29\%$	99.13 ± 0.00

Table 5: Results for $n = 1000$ experiments: The QD-score, coverage, and best solution after 10,000 iterations for each algorithm and domain with standard errors. Larger values are better across all metrics.

L ADDITIONAL RESULTS

L.1 Generated Archives and Additional Metrics

Table 6 presents the values of the QD-score, coverage, and best solution for each algorithm and domain. We used $\alpha = 0.01$ for CMA-MAE, identically to the main experiments. Similar to prior work [21], we disambiguate the quality of solutions found and coverage by showing for MAP-Elites, MAP-Elites (line), CMA-ME, and CMA-MAE the percentage of cells (y-axis) that have objective value greater than the threshold specified in the x-axis (Fig. 11).

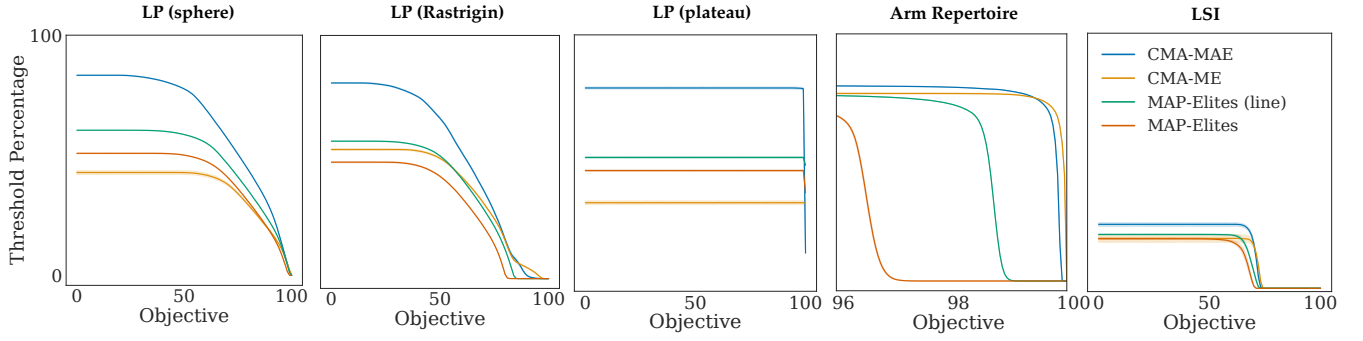


Figure 11: The percentage of cells in the y-axis with objective values larger than or equal to a threshold specified in the x-axis, with 95% confidence intervals. The percentage is the number of filled cells (filtered by the threshold) over the archive size. A larger area under each curve indicates better performance.

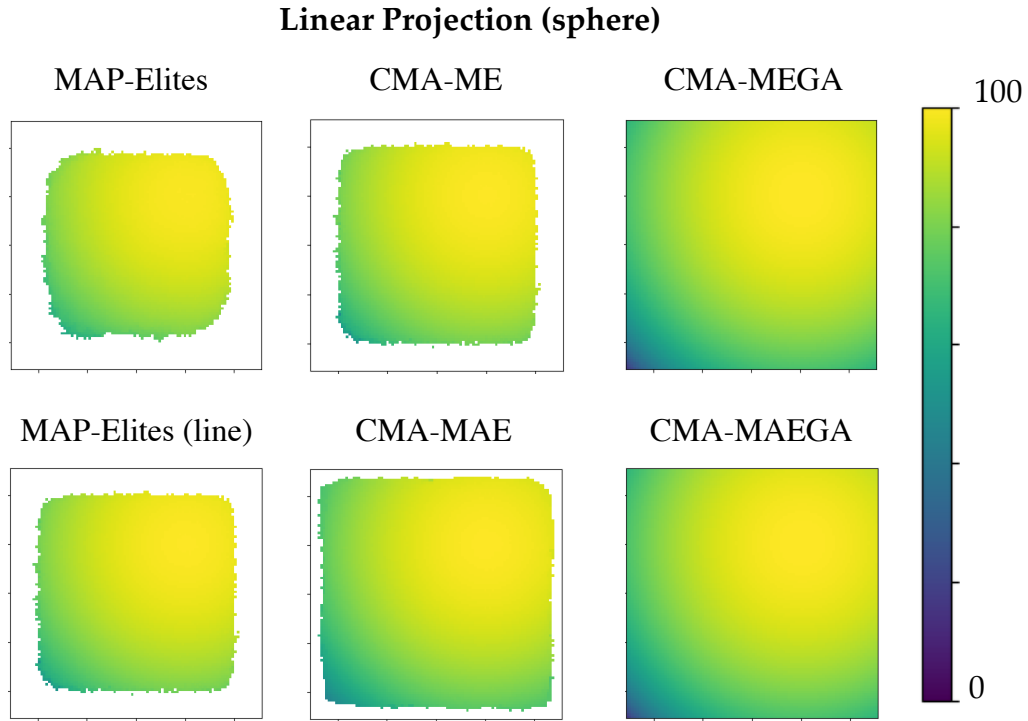


Figure 12: Example archives for each algorithm for the linear projection (sphere) domain.

L.2 Example Archives

Fig. 12 -16 show example archives for each algorithm and domain.

L.3 Additional Experiments in the LSI Domain

We include the same additional experiments in the LSI (StyleGAN) domain as prior work [21]. The first additional experiment has objective prompt “A photo of Jennifer Lopez” and measure prompts “A small child.” and “A woman with long blonde hair.” The second has objective prompt “A photo of Elon Musk” and measure prompts “A person with red hair.” and “A man with blue eyes.” Table 7 shows the results of the additional runs, as well as the Beyoncé run, with objective prompt “A photo of Beyoncé.”, from the main paper.

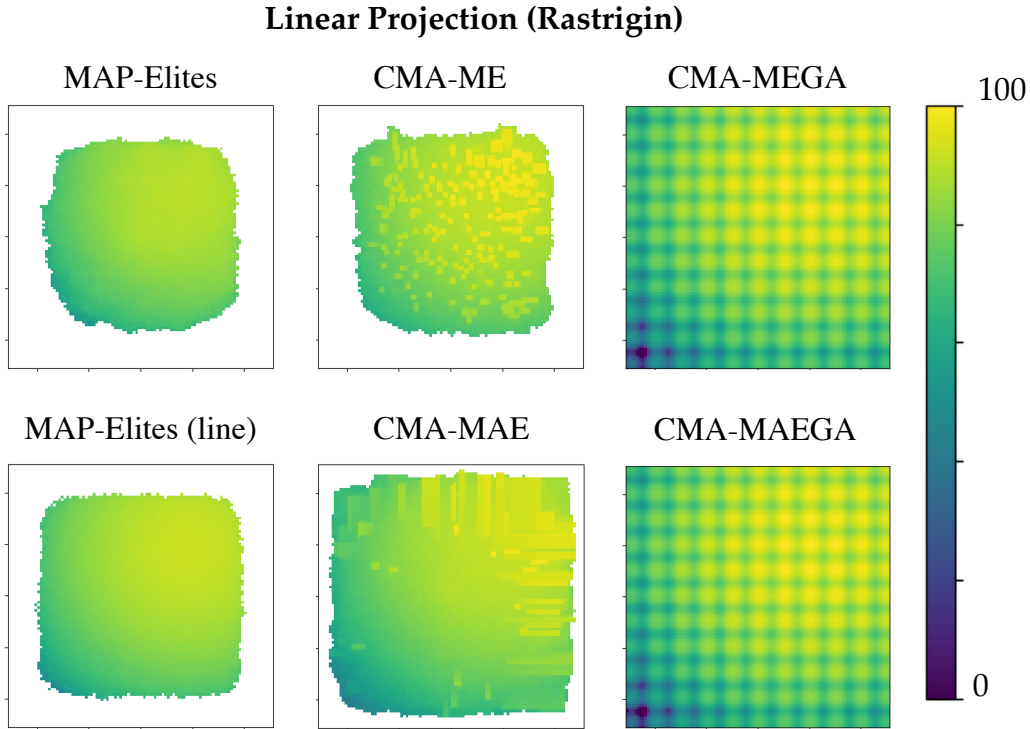


Figure 13: Example archives for each algorithm for the linear projection (Rastrigin) domain.

L.4 Additional Results for Varying Resolutions

Fig. 18 shows the QD-score and coverage of CMA-MAE with resolution-dependent archive learning rate and the baselines, for each benchmark domain. For CMA-MAE, we set the resolution dependent archive learning rate α using the conversion formula from Appendix G, with $\alpha_1 = 0.01$ for resolution 100×100 .

L.5 Qualitative Results in the LSI Domain

We present example collages for CMA-MAE (Fig. 20, 21), 19) and for CMA-MAEGA (Fig. 22, 23) for the LSI (StyleGAN) domain. We also include collages of each run of all algorithms for all runs of LSI (StyleGAN) and LSI (StyleGAN2) in the anonymous Dropbox link: https://www.dropbox.com/sh/7e22190k3p4zh69/AACcAKV7_Xgi4IMrhzxkCz5ca?dl=0.

M ETHICS STATEMENT AND SOCIETAL IMPACTS

By controlling the trade-off between exploration and exploitation in QD algorithms, we aim towards improving their performance and robustness, thus making these algorithms easier to apply in a wide range of domains and applications. One promising application is synthetically extracting datasets from generative models to train machine learning algorithms [3, 41]. This can raise ethical considerations because generative models can reproduce and exacerbate existing biases in the datasets that they were trained on [42, 58]. On the other hand, quality diversity algorithms with carefully selected measure functions can target diversity with desired attributes, thus we hypothesize that they can be effective in generating balanced datasets. Furthermore, by attempting to find diverse solutions, QD algorithms are a step towards open-endedness in AI [74] and will often result in unexpected and often surprising emergent behaviors [52]. We recognize that this presents several challenges in predictability and monitoring of AI systems [40], and we highlight the importance of future work on balancing the tradeoff between open-endedness and control [18].

N REPRODUCIBILITY INVENTORY

In the supplemental material we provide complete source code for all algorithms and experiments, as well as the Conda environments for installing project dependencies. The “README.md” document provides complete instructions both setup and execution of all experiments. In Appendix A we provide all hyperparameters. In Appendix B we provide domain-specific details for replicating all experimental domains. In Appendix C we provide information about the computational resources and hardware we used to run our experiments. In Appendix D we provide the pseudocode for the CMA-MAEGA algorithm, the DQD counterpart of CMA-MAE. In Appendix E we provide the proofs of all

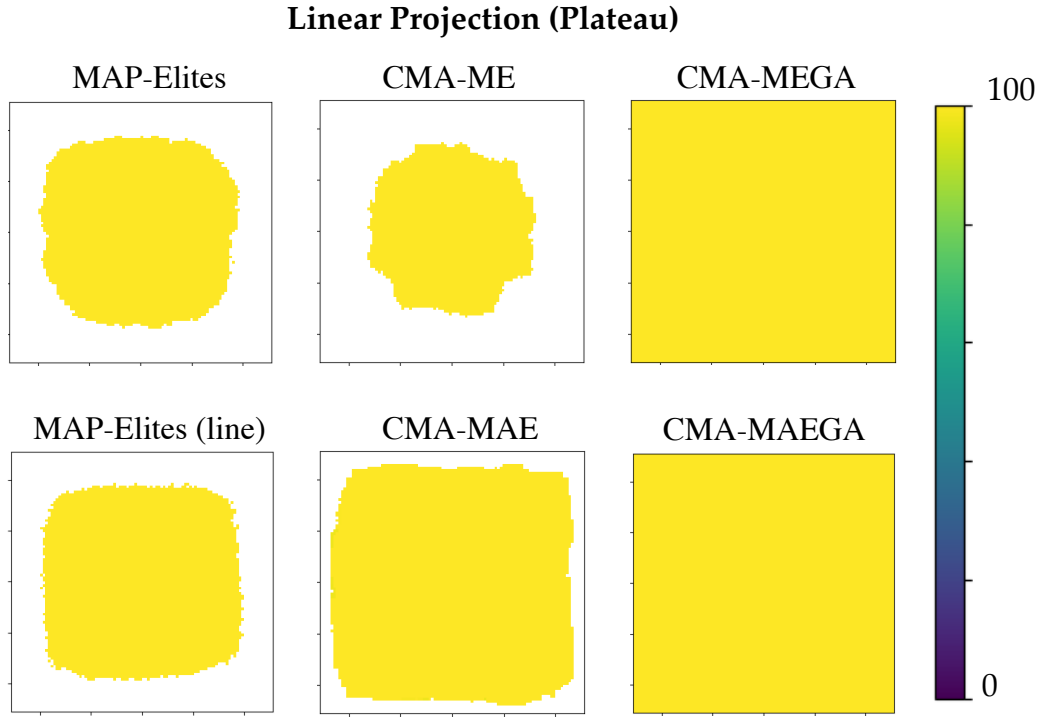


Figure 14: Example archives for each algorithm for the linear projection (plateau) domain.

theorems in the paper. In Appendix F we provide the theoretical properties of CMA-MAEGA. In Appendix G we provide the derivation of the conversion formula for the archive learning rate. In Appendix H we provide a batch threshold update rule that is invariant to the order that the solutions are processes within a batch update. In Appendix I we discuss the implementation details for additional experiments that improve the quality of the generated images in the latent space illumination domain. In Appendix L we present all metrics with standard errors for each algorithm and domain.

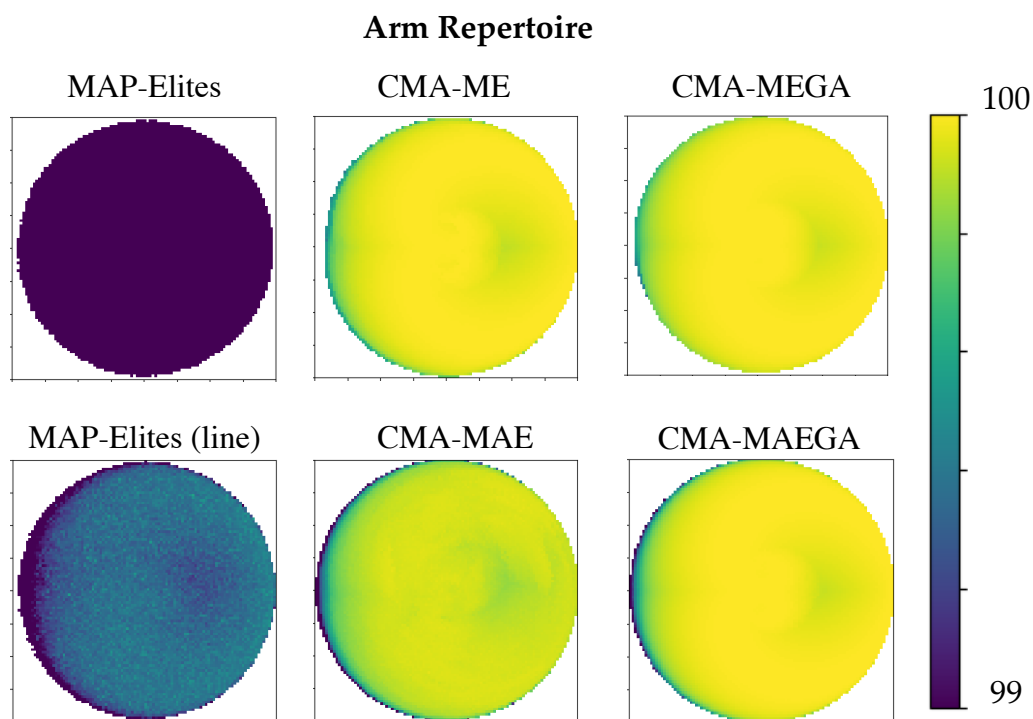


Figure 15: Example archives for each algorithm for the arm repertoire domain.

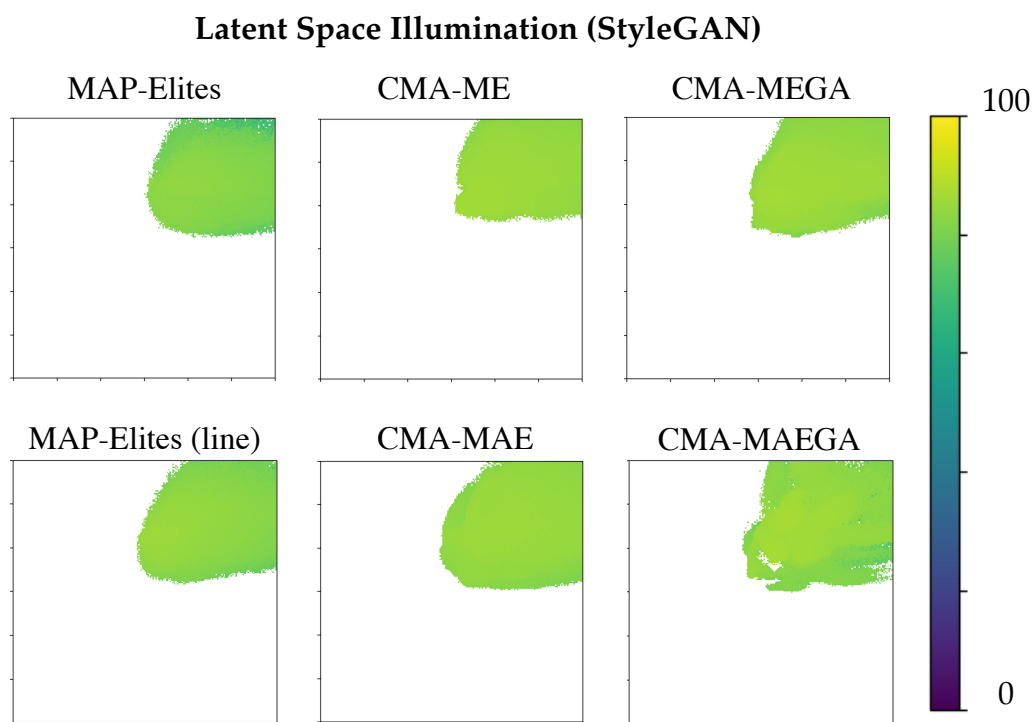


Figure 16: Example archives for each algorithm for the LSI (StyleGAN) domain.

Linear Projection (sphere)			
Algorithm	QD-score	Coverage	Best
MAP-Elites	41.64 \pm 0.06	50.80 \pm 0.09%	98.63 \pm 0.01
MAP-Elites (line)	49.07 \pm 0.03	60.42 \pm 0.05%	99.43 \pm 0.01
CMA-ME	36.50 \pm 0.31	42.82 \pm 0.40%	100.00 \pm 0.00
CMA-ME*	45.07 \pm 0.07	55.11 \pm 0.10%	99.23 \pm 0.02
CMA-ME (imp, opt)	37.10 \pm 0.37	43.62 \pm 0.45%	100.00 \pm 0.00
CMA-MAE	64.86 \pm 0.04	83.31 \pm 0.07%	99.59 \pm 0.01
CMA-MEGA	75.32 \pm 0.00	100.00 \pm 0.00%	100.00 \pm 0.00
CMA-MAEGA	75.39 \pm 0.00	100.00 \pm 0.00%	100.00 \pm 0.00
Linear Projection (Rastrigin)			
Algorithm	QD-score	Coverage	Best
MAP-Elites	31.43 \pm 0.07	47.88 \pm 0.12%	82.16 \pm 0.11
MAP-Elites (line)	38.29 \pm 0.05	56.51 \pm 0.09%	85.71 \pm 0.07
CMA-ME	38.02 \pm 0.11	53.09 \pm 0.16%	97.59 \pm 0.06
CMA-ME*	35.06 \pm 0.05	53.01 \pm 0.12%	83.47 \pm 0.08
CMA-ME (imp, opt)	34.87 \pm 0.24	48.93 \pm 0.40%	98.18 \pm 0.03
CMA-MAE	52.65 \pm 0.06	80.46 \pm 0.11%	95.90 \pm 0.25
CMA-MEGA	63.07 \pm 0.00	100.00 \pm 0.00%	100.00 \pm 0.00
CMA-MAEGA	63.06 \pm 0.00	100.00 \pm 0.00%	100.00 \pm 0.00
Linear Projection (plateau)			
Algorithm	QD-score	Coverage	Best
MAP-Elites	47.07 \pm 0.17	47.07 \pm 0.17%	100.00 \pm 0.00
MAP-Elites (line)	52.20 \pm 0.19	52.20 \pm 0.19%	100.00 \pm 0.00
CMA-ME	34.54 \pm 0.35	34.54 \pm 0.35%	100.00 \pm 0.00
CMA-ME*	51.11 \pm 0.25	51.11 \pm 0.25%	100.00 \pm 0.00
CMA-ME (imp, opt)	31.91 \pm 0.43	31.91 \pm 0.43%	100.00 \pm 0.00
CMA-MAE	79.27 \pm 0.21	79.29 \pm 0.21%	100.00 \pm 0.00
CMA-MEGA	100.00 \pm 0.00	100.00 \pm 0.00%	100.00 \pm 0.00
CMA-MAEGA	100.00 \pm 0.00	100.00 \pm 0.00%	100.00 \pm 0.00
Arm Repertoire			
Algorithm	QD-score	Coverage	Best
MAP-Elites	71.40 \pm 0.03	74.09 \pm 0.04%	97.38 \pm 0.03
MAP-Elites (line)	74.55 \pm 0.02	75.61 \pm 0.02%	99.16 \pm 0.01
CMA-ME	75.82 \pm 0.11	75.89 \pm 0.11%	100.00 \pm 0.00
CMA-ME*	75.68 \pm 0.04	76.13 \pm 0.03%	99.78 \pm 0.01
CMA-ME (imp, opt)	75.91 \pm 0.07	75.99 \pm 0.07%	100.00 \pm 0.00
CMA-MAE	79.03 \pm 0.02	79.24 \pm 0.02%	99.93 \pm 0.00
CMA-MEGA	75.21 \pm 0.13	75.25 \pm 0.13%	100.00 \pm 0.00
CMA-MAEGA	79.27 \pm 0.02	79.35 \pm 0.02%	100.00 \pm 0.00
Latent Space Illumination (StyleGAN)			
Algorithm	QD-score	Coverage	Best
MAP-Elites	12.85 \pm 0.10	19.42 \pm 0.16%	71.42 \pm 0.14
MAP-Elites (line)	14.40 \pm 0.09	21.11 \pm 0.11%	73.04 \pm 0.05
CMA-ME	14.00 \pm 0.62	19.57 \pm 0.90%	74.11 \pm 0.08
CMA-MAE	17.67 \pm 0.27	25.08 \pm 0.40%	73.48 \pm 0.18
CMA-MEGA	16.08 \pm 0.37	22.58 \pm 0.57%	74.95 \pm 0.27
CMA-MAEGA	16.20 \pm 0.41	23.83 \pm 0.46%	75.52 \pm 0.22
Latent Space Illumination (StyleGAN2)			
Algorithm	QD-score	Coverage	Best
MAP-Elites	-276.18 \pm 32.00	4.48 \pm 0.18%	-936.96 \pm 35.91
MAP-Elites (line)	-827.25 \pm 25.99	8.81 \pm 0.04%	-236.65 \pm 13.35
CMA-MEGA	9.18 \pm 0.18	14.91 \pm 0.12%	67.48 \pm 0.09
CMA-MAEGA	11.51 \pm 0.09	18.62 \pm 0.16%	66.17 \pm 0.08

Table 6: Results: The QD-score, coverage, and best solution after 10,000 iterations for each algorithm and domain with standard errors. Larger values are better across all metrics.

Latent Space Illumination (StyleGAN2)

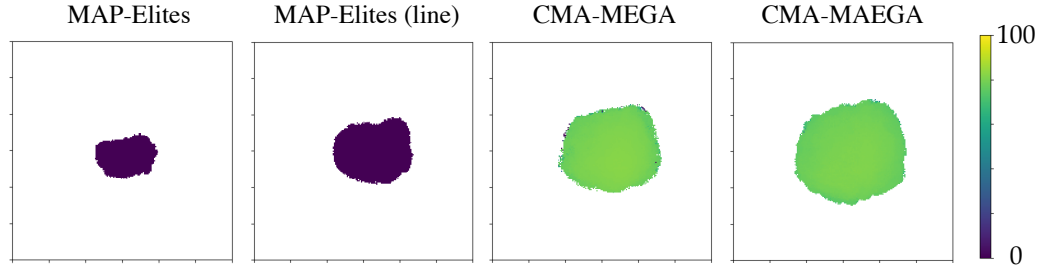


Figure 17: Example archives for each algorithm for the LSI (StyleGAN2) domain.

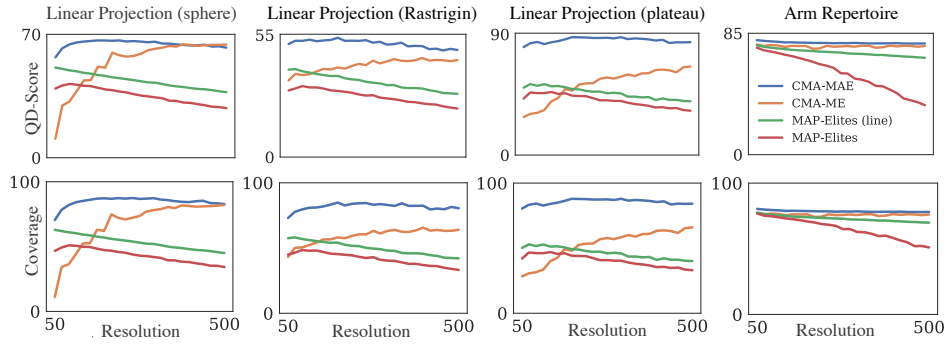


Figure 18: Final QD-score and coverage of each algorithm for 25 different archive resolutions.

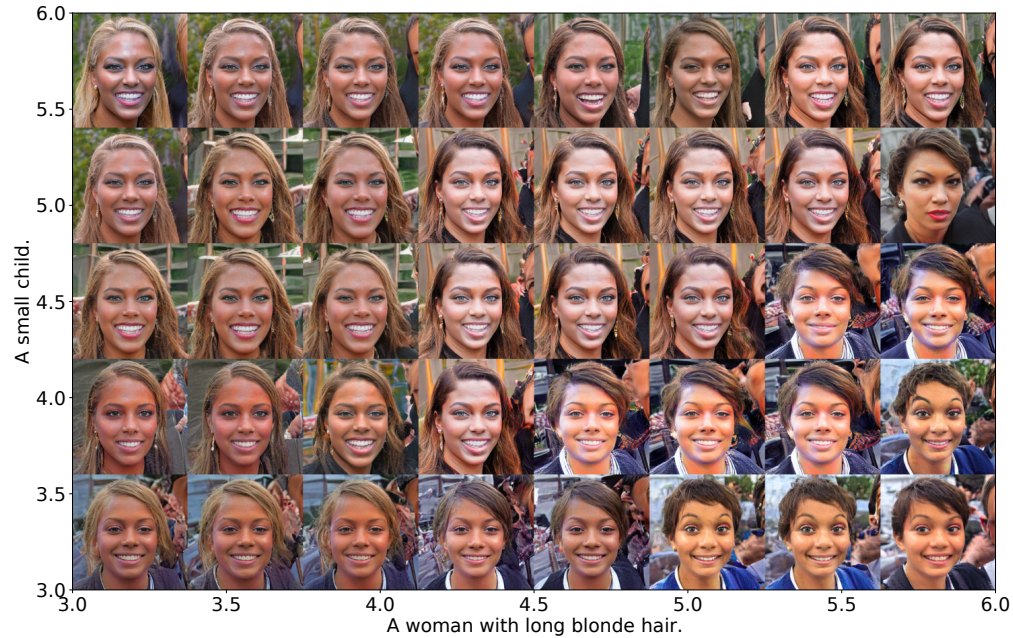


Figure 19: A latent space illumination collage generated by CMA-MAE for the objective “A photo of Beyonce.” and for measures “A small child.” and “A woman with long blonde hair.” The axis values indicate the score returned by the CLIP model, where lower score indicates a better match.

LSI (StyleGAN): Beyoncé			
Algorithm	QD-score	Coverage	Best
MAP-Elites	12.85 ± 0.10	$19.42 \pm 0.16\%$	71.42 ± 0.14
MAP-Elites (line)	14.40 ± 0.09	$21.11 \pm 0.11\%$	73.04 ± 0.05
CMA-ME	14.00 ± 0.62	$19.57 \pm 0.90\%$	74.11 ± 0.08
CMA-MAE	17.67 ± 0.27	$25.08 \pm 0.40\%$	73.48 ± 0.18
CMA-MEGA	16.08 ± 0.37	$22.58 \pm 0.57\%$	74.95 ± 0.27
CMA-MAEGA	16.20 ± 0.41	$23.83 \pm 0.46\%$	75.52 ± 0.22
LSI (StyleGAN): Jennifer Lopez			
Algorithm	QD-score	Coverage	Best
MAP-Elites	12.51 ± 0.28	$19.18 \pm 0.48\%$	70.87 ± 0.27
MAP-Elites (line)	14.73 ± 0.06	$21.60 \pm 0.08\%$	73.50 ± 0.13
CMA-ME	15.24 ± 0.37	$20.86 \pm 0.50\%$	75.39 ± 0.09
CMA-MAE	18.33 ± 0.16	$25.42 \pm 0.24\%$	75.10 ± 0.17
CMA-MEGA	17.06 ± 0.10	$23.40 \pm 0.14\%$	76.02 ± 0.08
CMA-MAEGA	16.45 ± 0.27	$23.60 \pm 0.49\%$	76.42 ± 0.13
LSI (StyleGAN): Elon Musk			
Algorithm	QD-score	Coverage	Best
MAP-Elites	13.88 ± 0.11	$23.15 \pm 0.14\%$	69.76 ± 0.07
MAP-Elites (line)	16.54 ± 0.28	$25.73 \pm 0.31\%$	72.63 ± 0.28
CMA-ME	18.96 ± 0.17	$26.18 \pm 0.24\%$	75.84 ± 0.10
CMA-MAE	22.10 ± 0.31	$30.89 \pm 0.44\%$	75.25 ± 0.20
CMA-MEGA	21.82 ± 0.18	$30.73 \pm 0.15\%$	76.89 ± 0.15
CMA-MAEGA	19.99 ± 0.21	$30.12 \pm 0.42\%$	77.25 ± 0.18

Table 7: Results from additional runs for Beyoncé, Jennifer Lopez, and Elon Musk

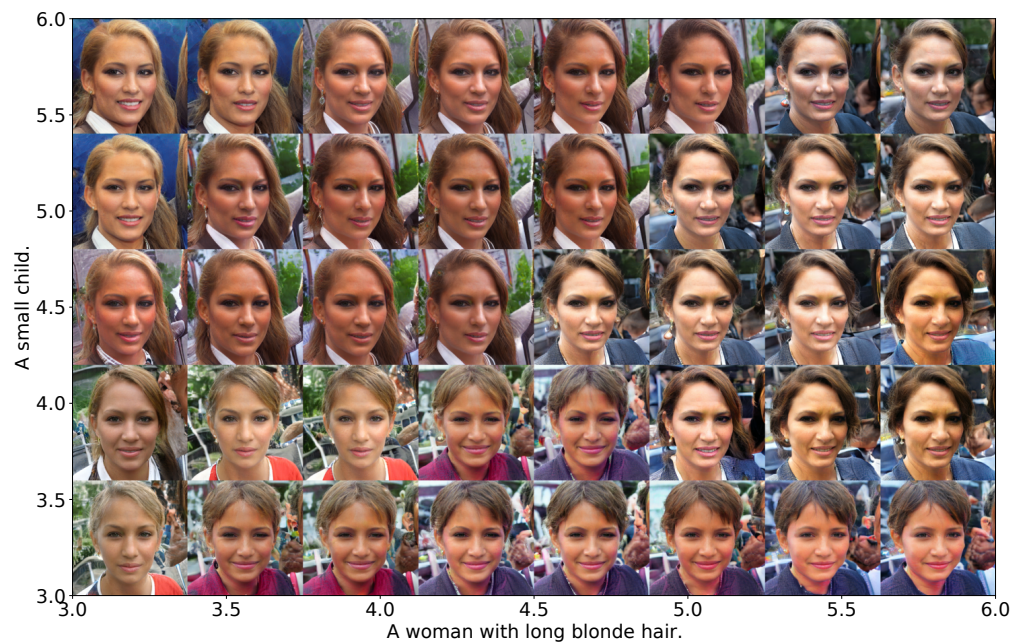


Figure 20: A latent space illumination (StyleGAN) collage generated by CMA-MAE for the objective “A photo of Jennifer Lopez.” and for measures “A small child.” and “A woman with long blonde hair.” The axes values indicate the score returned by the CLIP model, where lower score indicates a better match.

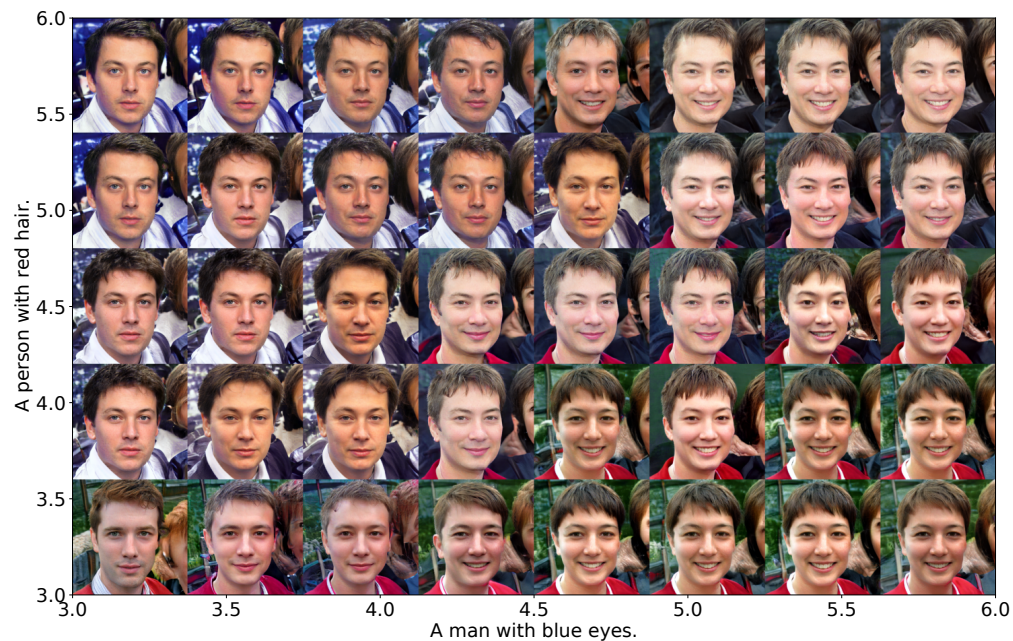


Figure 21: A latent space illumination (StyleGAN) collage generated by CMA-MAE for the objective “Elon Musk with short hair.” and for measures “A man with blue eyes.” and “A person with red hair.” The axes indicate the score returned by the CLIP model, where lower score indicates a better match.

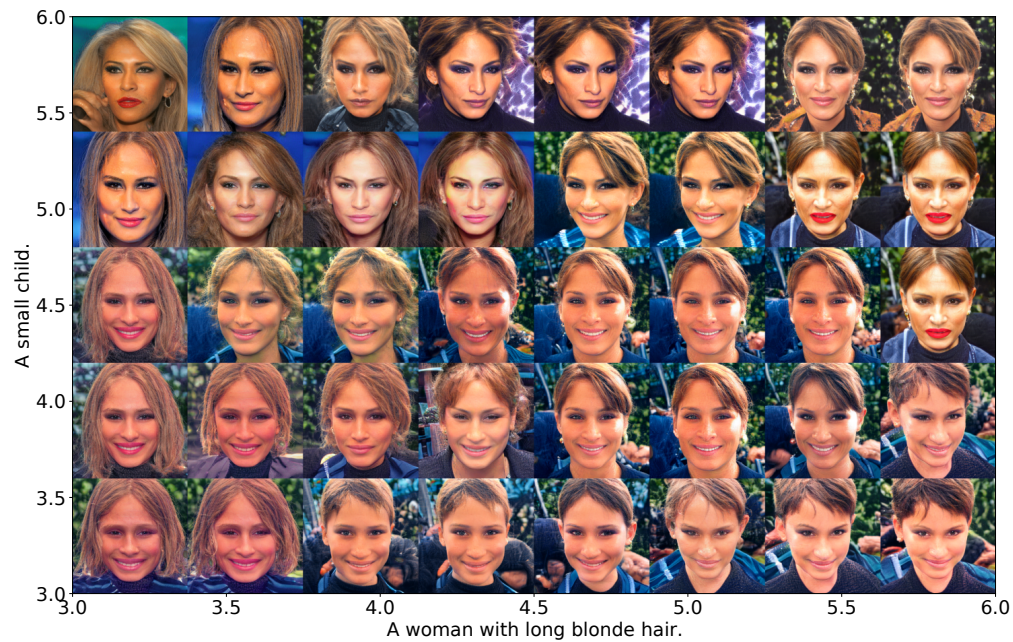


Figure 22: A latent space illumination (StyleGAN) collage generated by CMA-MAEGA for the objective “A photo of Jennifer Lopez.” and for measures “A small child.” and “A woman with long blonde hair.” The axes values indicate the score returned by the CLIP model, where lower score indicates a better match.

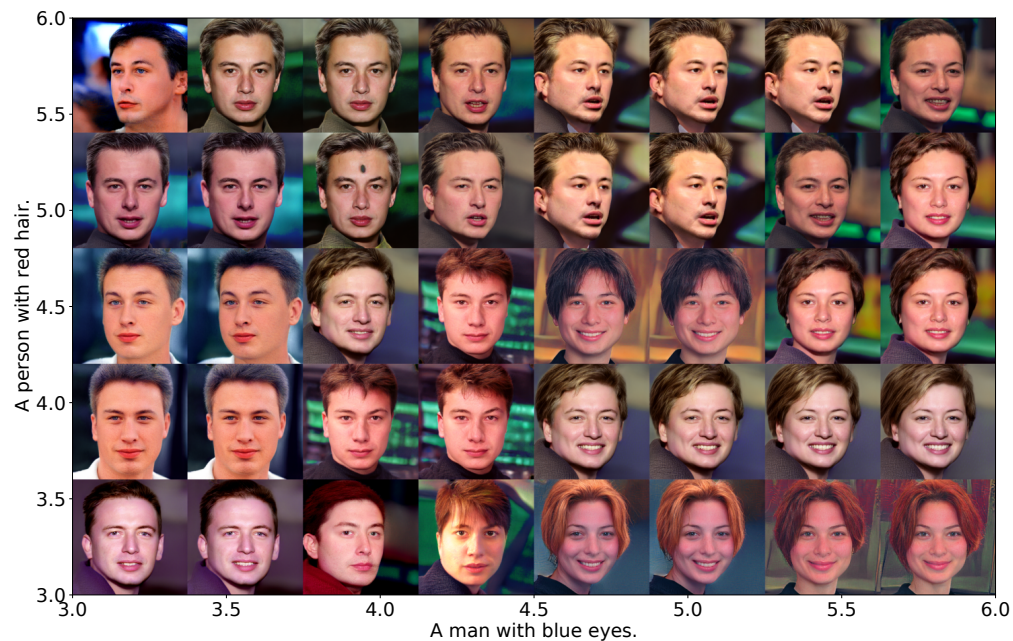


Figure 23: A latent space illumination (StyleGAN) collage generated by CMA-MAEGA for the objective “Elon Musk with short hair.” and for measures “A man with blue eyes.” and “A person with red hair.” The axes values indicate the score returned by the CLIP model, where lower score indicates a better match.